DR. RAMON MERCEDES-MARTÍN (Orcid ID : 0000-0002-4410-1984)

DR. MIKE ROGERSON (Orcid ID : 0000-0001-6016-0549)

Article type : Original Research Article

Effects of Salinity, Organic Acids and Alkalinity in the Growth of Calcite Spherulites: Implications for Evaporitic Lacustrine Sedimentation

Ramon Mercedes-Martín[1*], Ashit Rao[2], Mike Rogerson[3], and Mónica Sánchez-Román[4]

1*. SZALAI Grup S.L., P.O Box 1005, Caimari, 07314, Spain (* info@ramonmercedes.com)

2. Faculty of Science and Technology (TNW), Physics of Complex Fluids (PCF), University of Twente, 7522 NB, Enschede, The Netherlands.

3. Department of Geography and Environmental Science, Ellison Building, Northumbria University, Newcastle, NE1 8ST

4. Vrije Universiteit Amsterdam, Earth Sciences Department, Faculty of Science. De Boelelaan 1086, 1081 HV, Amsterdam, The Netherlands.

ABSTRACT

Lacustrine non-skeletal carbonates exhibit a diversity of petrographies due to interactions between physico-chemical and biologically influenced mechanisms. Despite the suggestion that evaporative concentration was involved in the formation of spherulite and shrubby-bearing carbonate successions in the Pre-Salt Cretaceous alkaline lakes of the South Atlantic, no consensus exists about the water chemistries promoting these exotic mineral textures. In this work, an

This article has been accepted for publication and undergone full peer review but has not been through the copyediting, typesetting, pagination and proofreading process, which may lead to differences between this version and the Version of Record. Please cite this article as doi: 10.1002/DEP2.136

experimental approach was developed to evaluate how changes in salinity (NaCl) and biopolymer concentrations (alginic acid) impact calcite growth dynamics from saline and alkaline synthetic solutions. Hydrochemical and petrographical data from selected modern saline/ alkaline environments was compared with experimental datasets to further estimate how the underlying (bio)chemical conditions and lake locations likely converge to allow the formation of calcite spherulite grains in evaporitic settings. Spherulitic calcite from Recent saline lakes and experiments arise from waters with moderate to high [Calcium]/[Alkalinity] ratios ([Ca]/[Alk]) rather than in calcium-depleted and alkaline-rich environments which tend to produce single-crystal calcites during abiotic water mixing or lake evaporation. This is consistent with the assembly of polycrystalline textures being a kinetically controlled feature, forced by remarkably high rates of nucleation. Also, the data analysed do not support a causative relationship between evaporite-driven salinity fluctuations and the preferential formation of spherulites, shrubs or their intermediate textures. Ubiquitous in saline lakes, organic substances can lower the kinetic thresholds for spherulitic calcite aggregation while microbial photosynthesis can also raise pH, altogether enhancing calcite supersaturation and promoting spherulite formation in waters with moderate-high [Ca]/[Alk] ratios and high salinities. Localised observations of abiotic spherulites in Recent soda lakes can occur in restricted mixing zones where [Ca]/[Alk] ratios are enhanced. This work highlights the roles of concentration regimes associated with biopolymers and microbial metabolism against the background salinity fluctuations in determining the morphological and textural transitions in lacustrine carbonate minerals.

Keywords: alginic acid, alkaline, calcite, evaporation, salinity, shrub, spherulite

1. INTRODUCTION

One of the longstanding conundrums in sedimentology lies in how to demarcate the influences exerted by abiotic processes and biologically influenced mechanisms in the formation and early diagenesis of non-skeletal carbonates (Serebryakov, 1976; Wilkinson and Given, 1986; Kelts and Talbot, 1990; Webb, 1996; Bosak et al., 2004; Stalport et al., 2005; McLoughlin, et al, 2007; Morse et al., 2007; Sánchez-Román et al., 2008, 2011; Rainey and Jones, 2009; Wacey, 2010;

Fouke, 2011; Wright, 2012; Sánchez-Navas et al., 2013; Capezzuoli et al., 2014; Brasier et al., 2015). It is still necessary to unify criteria to evaluate whether non-enzymatic carbonates have a biogenic influence, or whether they can form totally abiotically. This problem remains one of the most fundamental in sedimentology, critically conditioning models of how life has impacted substrate formation, lithification, and diagenesis on Earth (Hodgson et al., 2018). Moreover, this issue permeates through the recognition of early life signatures on Earth and in our solar system (Brasier et al, 2015; Chan et al., 2019).

On Earth, continental environments form incredibly diverse associations of micron-sized carbonate crystals comprising different mineralogies and fabrics (Jones, 1994; 2017; Frisia et al., 2000; Taylor and Chafetz, 2004; Jones and Renaut, 1995; Pedley et al., 2009; Sánchez-Román et al., 2009; Sanz-Montero et al., 2019; Jones and Peng, 2014; Capezzuoli et al., 2014), thus representing excellent sites to evaluate whether crystal morphogenesis arises from physical, chemical or biological processes or a combination of them.

More recently, this debate has focussed on the origin of some enigmatic but abundant carbonate textures forming the Cretaceous Pre-Salt hydrocarbon reservoirs of the South Atlantic margins (Luiz-Dias, 2005; Terra et al., 2010; Wright, 2012; Muniz and Bosence, 2015; Mercedes-Martín et al., 2016, 2019; Gomes et al., 2020) (Figure 1A, B). These carbonates have been described as constituted by the recurrent combination of two morphological end-members: fibro-radial polycrystalline calcite spherulites and upward bifurcating and dense radiating, fibrous to bladed, fascicular-optic to radial-fibrous, polycrystalline shrubs (Terra et al., 2010; Wright and Barnett, 2015; Saller et al., 2016; Herlinger et al., 2017; Farias et al., 2019; Gomes et al., 2020) (Figure 1A, B).

The close association of these carbonates with authigenic Mg-rich clays such as stevensite, talc or kerolite, the scarcity of voluminous sulphate deposits, and the apparent lack of marine fossils have been interpreted as indicative of highly evaporitic settings commonly associated with saline lacustrine environments (Wright and Barnett, 2015; Tosca and Wright, 2015; Saller et al., 2016; Farias et al., 2019; Lima and Ros, 2019). Mineral assemblages found in these lakes strongly advocate for alkaline environments with elevated pH, Mg/Si ratios as well as salinity (Tosca and Masterson, 2014; Tosca and Wright, 2015; Tutolo and Tosca, 2018). The interpretation that Mg-silicate precipitation arose from evaporative concentration over extensive lacustrine areas (Jones,1986; Darragi and Tardy, 1987; Deocampo and Renaut, 2016) has favoured the view that Pre-Salt minerals formed in waters containing only modest concentrations of Ca^{2+} and Mg^{2+} ions

while being net alkaline systems with initial $[Ca^{2+}]/[CO_3^{2-} + HCO_3^{2-}]$ ratios less than 0.5 (Tutolo and Tosca, 2018). However, although such voluminous polycrystalline carbonate formations are likely unique, materials with these polycrystalline characteristics are not rare, being found in a range of terrestrial environments (Erthal et al., 2017; Chaftez et al 2018). These terrestrial settings generally exhibit biological influence on precipitation and occur in calcium-rich systems fed by meteoric waters. Spherulites very comparable to the Pre-Salt are reported from hyperalkaline springs with high calcium concentrations, where they contact with the atmosphere consuming large masses of $CO_{2(g)}$ enabling extensive carbonate-clay-silica precipitation (Chavagnac et al, 2013; Rogerson et al., 2017).

Earlier models interpreted the Pre-Salt lacustrine mineral morphologies and facies successions as generated by successive cycles of lake evaporation and refilling (Wright and Barnett, 2015), prompting specific 'chemical divides' (*sensu* Eugster and Hardie, 1978) and allowing critical mineral precipitation events. According to Wright and Barnett (2015), the progressive evaporation of lake waters promoted the successive formation of authigenic Mg-clays, followed by spherulite growth within clay gels, and finally the development of crystal dendrite shrubs in areas of reduced clay presence (Wright and Barnett, 2015; Wright and Tosca, 2016) (Figure 1C, D). An alternative evaporitic model by Farias et al., (2019), also based on the chemical divides of Eugster and Hardie (1978), suggested the following facies patterns: i) formation of calcite shrubs associated with evaporative concentration stages in flooded lake areas, and ii) subsequent calcite spherulite and Mg-rich clay deposition, generated displacively within the unconsolidated muddy sediment during desiccation stages.

Models by Wright and Tosca (2016) and Farias et al. (2019) imply that increased evaporation follows the preferential formation of shrubs over spherulites (Wright and Barnett, 2015), or spherulites over shrubs (Farias et al., 2019). These models assume that lacustrine carbonate precipitation is an abiotic and thermodynamically forced process triggered by evaporative-induced chemical divides (Figure 1C, D). As illustrated in their thermodynamic model (Figure 1C), Wright and Tosca (2016) assume that calcite/ stevensite precipitation takes place in equilibrium during the evaporation trajectory while a progressive rise in sodium and chloride solute concentrations occurs (see Figure 1C). However, this model overlooks a finding of crystal engineering research that polycrystalline precipitation reflects kinetic rather than thermodynamic forcing (Sunagawa, 1999), and the repeated observation that the millimetre-sized spherulites developing today are associated with biological influences (Chafetz et al., 2018, Bischoff et al., 2020).

The absence of Recent alkaline saline lakes precipitating quantitatively abundant spherulite-shrub facies prevents a detailed evaluation of the intricate biotic-influenced/ abiotic parameters involved in the formation of these carbonates. This conundrum undermines our ability to delineate the parameter space and depositional processes governing the formation of intermediate morphologies between spherulites and shrubs (Figure 1A, B; Gomes et al., 2020). This reflects a serious knowledge gap in understanding the origin and diagenesis of lacustrine carbonates in alkaline, saline settings.

The purpose of the present work is to investigate the conditions promoting or inhibiting calcite spherulite and shrub formation by comparing laboratory observations with data from alkaline saline lakes, following a heuristic methodology. Comparisons between hydrochemical data from Recent spherulite-producing alkaline and/or saline lakes, with data from lakes that are not known to precipitate spherulitic carbonates were made with the purpose of relating petrography with lake water chemistry. In addition, an experimental set-up was designed to test whether calcite spherulite growth morphology could be altered by salinity fluctuations driven by evaporative concentration. To this end, the effects of increased evaporation (i.e., rise in sodium and chloride in solution) were simulated while keeping other variables essentially constant (i.e., calcite saturation index and [Calcium]/ [Alkalinity] in solution) (Figure 1C). By combining hydrochemical data from the natural lacustrine systems and laboratory scale experiments, it is possible to explore and discuss the links between salinity, [Calcium]/ [Alkalinity] and organic acids (indicative of microbial metabolism) in the formation of calcite spherulites and shrubby calcite in lacustrine evaporitic settings.

2. METHODS AND MATERIALS

2.1. Parental batch preparation

Parental solutions were synthetically prepared to be comparable in terms of alkalinity to Mono Lake waters (Connell and Dreiss 1995), a saline, alkaline lake system located in Sierra Nevada (California) (Table S1). All experiments were prepared in a stainless steel horizontal laminar flow cabinet equipped with a UV-C lamp to prevent external contamination. The parental solution was prepared by adding powdered/ pearl reagent-grade anhydrous Ca $(OH)_2$, together with NaCl, Mg $(OH)_2$, Na_2SiO_3 and H_3BO_3 to deionised water (18 MΩ-cm). In order to investigate the effects of salinity and evaporative gradients, two types of parental solutions were prepared: a low salinity

solution with 2.08 g/L NaCl (experiments 1 and 2) and a high salinity solution with 10.40 g/L of NaCl (experiments 3 and 4) (Table S1 and S2). In all experiments, a soda stream mechanism was used to bubble equal amounts of CO_2 into the parental solutions. To achieve sterility, powdered chemicals, frosted glass slides, tweezers, and glassware were heat-sterilised by autoclave at 160°C for two hours. Deionised water was then autoclaved in an ASTELL Sterilizer at a maximum of 121°C and 1700 millibars for two hours. Items that could not be heat-sterilised, such as tubing and plastic pipette tips, were treated with 16% hydrogen peroxide solution overnight.

2.2. Experimental set-up of alkaline synthetic waters

The pH values of the parental solutions were subsequently adjusted to 12 by the addition of NaOH pellets. Once the targeted pH was confirmed using a glass-bodied Jenway 3510 pH meter electrode, aliquots were redistributed and essayed in 100 ml conical glass flasks (four flasks per experiment) which contained sterilised 1 cm^2 frosted glass slides. The flask filling process was carried out using sterile 0.22 µm diameter MF-Millipore filters to remove any contaminant particulates or pre-existing crystals which could have formed in the parental solutions. Initial alkalinities were systematically measured using a Mettler-Toledo T50 digital titrator and a DGi117-water pH electrode with a Rondolino autosampler (Table 1 and S2). After this stage, only experiments 2 and 4 were filled with 1 mg/L of sterile alginic acid, a common organic molecule from microbial cell walls. After alkalinity measurements, all the flasks from experiments 1 to 4 were sealed and agitated in an orbital flask shaker at 125 rpm. Continuous agitation ensures mixing of reactants while the experiments ran for 3 days at room temperature (about 25°C) in a controlled environment cabinet under dark conditions.

2.3. Sampling and microscopic observations

After three days the solutions and precipitates were sampled. Frosted slides were oven-autoclaved at 100°C for one hour. Crystals precipitated in the bottom of the flasks were collected using a Büchner glass funnel with integrated sterilised cellulose nitrate filters (0.2 µm), which were autoclaved at 45°C for 1 hour. Frosted slides were removed from the flasks by using sterilised tweezers. Dried slides and friable material were placed on aluminium stubs, carbon coated and observed with a Zeiss EVO60 and JEOL J-7100F scanning electron microscope (SEM). The SEM imaging and measurements were performed at beam currents of *ca* 40 µA and *ca* 20 kV EHT accelerating voltage. Elemental X-ray analyses were also conducted with an Inca System350

Energy Dispersive X-ray Spectrometer (EDX). X-ray powder diffraction data was collected from the glass slides with crumbly material mounted in stainless steel sample holders. Measurements were performed between 20 and 50 degrees (2Θ range) on solids. A PANalytical Empyrean diffractometer operating in Bragg-Brentano geometry with copper $K\alpha_1$ (λ = 1.540546 Å) and a PIXEL detector was used for data collection.

Elemental (Ca, Mg and Na) concentrations were measured using a Perkin Elmer Optima 5300DV inductively coupled optical emission spectrometer (ICP-OES). Selection of the analytical lines was based on the Perkin Elmer recommendations for the Optima 5300DV spectrometer, 393.366 nm for calcium and 280.271 nm for magnesium, and 589.562 nm for sodium. Calibration standards were prepared using 1,000 ppm standard stock solutions (99.9% pure or greater, PrimAg, Xtra, Romil, Cambridge) of calcium and magnesium. Samples were diluted with 5% ultrapure HNO_3 to bring the expected concentrations within or near to the linear calibration of the standards. Saturation indexes (SI) of calcite and sepiolite, solution ionic strengths, $[Ca^{2+}]$ and $[CO_3^{2-}]$ activities and $[Ca^{2+}]/[CO_3^{2-}]$ ratios of the initial and final solutions were calculated using the geochemical software PHREEQC (Parkhurst and Appelo, 2013). Furthermore, calcium and magnesium average removal rates from solutions were estimated (Table S2).

2.4. Compilation of hydrochemical data from Recent saline lakes and experiments

A literature review on six Recent saline lakes/ lagoons was carried out to analyse the potential links between salinity, [Calcium]/[Alkalinity] ratios (expressed as [Ca]/[Alk]), metal ion concentrations, and the carbonate products observed, either in the form of water column precipitates, loose sediments, or benthic microbial-related deposits (Table 1). Lakes were selected on the basis of the previously documented occurrence of spherulite calcite grains or polycrystalline calcite textures that could plausibly have formed contemporaneously with recent lake waters (Kiritimati atoll lake, Rottnest lagoon, or Great Salt Lake). Comparisons were also made with other saline lakes/ lagoons where such textures are unknown (Mono Lake, Lake Van, and Lake Clifton). Values of salinity (g/L); alkalinity (meq/L); pH; Mg/Ca ratio; calcium and magnesium concentrations (meq/L); and [Ca]/ [Alkalinity] ratios were gathered from the available literature when possible. Measurements come from surficial lake/lagoon water locations if not stated otherwise. Salinity is referred to the sum of [Na] and/or [Cl] concentrations either measured in the waters or calculated using PHREEQC geochemical software (Parkhurst and Appelo, 2013).

Limitations exist when relating lake water chemistry with Recent carbonate microfabrics and additional parameters including DOC, sulphate, phosphate, or trace element concentrations may influence carbonate precipitation and morphology. Also, the chemistry of the lake sediment-water interface can differ from that of the water column. However, all of these influences would also cause deviation from a simple evaporation-forced scenario, and so do not undermine the evaluation. By comparing data from experiments and saline lakes, certain chemical scenarios emerge more favourable to the development of specific carbonate microfabrics than others. To ensure that the dataset was representative, samples from a range of hydrological settings were included. Hydrochemical data from previous experimental works addressing spherulite calcite growth on the laboratory scale was also included.

2.5. Terminology

Abiotic precipitation. Considered here to be calcite products precipitated due to inorganic physico-chemically forced processes with no influence of organic molecules, microbial exopolymeric substances or microbial metabolisms (see Gallagher et al., 2010).

Biotically-influenced precipitation. Defined here as calcite products precipitated under the influence of organic molecules, microbial exopolymeric substances or microbial metabolisms (see Gallagher et al., 2010). Biomolecules can mediate in the transformation process between amorphous calcium carbonate phases and crystalline solids such as calcite, or aragonite (Addadi et al., 2003; Ma and Feng, 2015).

Single crystal refers here to a crystalline solid in which the crystal lattice of the entire sample is continuous and unbroken to the edge of the sample, with no grain boundaries (Meldrum and Cölfen, 2008; Zhou and O'Brien, 2008). In most instances, single crystals are characterised by a regular internal structure with smooth and planar external faces (Meldrum and Cölfen, 2008); however, single crystals with curved surfaces are also formed in nature (e.g. biominerals) where crystals grow in the presence of organic substances (Young et al, 1999; Meldrum and Cölfen, 2008).

Polycrystal refers to polycrystalline solids formed of aggregates of numerous grains or elongated crystallites representing the basic crystallographic units (Cölfen and Antonieti, 2008; Imai, 2016). Polycrystals can grow through the random aggregation of small 'crystal building blocks' (Imai, 2016).

Calcite spherulites or *Spherulitic calcite* refer here to spherical to dumbbell-shaped calcite solids internally constituted by a clear polycrystalline arrangement. Consequently, calcite spherical solids not showing such internal architecture were not considered in this study.

Shrubby calcite is described here as upward bifurcating and dense radiating, fibrous and polycrystalline calcite solids, either microscopic or macroscopic.

Benthic microbial textures encompass those microscopic to macroscopic carbonate components that have formed in close spatial association with microbial communities and/or their exopolymers at the water-sediment interface giving rise to static substrates/crusts (e.g. tufa towers, pinnacles, mounds, microbialites).

Microbialite or *microbial deposit* refers here to organo-sedimentary macroscopic carbonate deposits that have accreted as a result of a benthic microbial community trapping and binding detrital sediment and/or forming the locus of mineral precipitation *sensu* Burne and Moore (1987).

3. RESULTS

The hydrochemical and petrographic data from the batch experiments 1 to 4 are summarised in Figure 2, with the respective crystalline solids illustrated in Figures 3 through 6. The experimental data presented here are compared with the microscale carbonate products and hydrochemical parameters from the studied alkaline, saline lakes and previous experimental works (summarised in Table 1).

3.1. Experiment 1: Low Salinity and Without Organic Acids

Mineralisation experiments performed with salinity equivalent to 2.08 g/L NaCl and devoid of organic acids produced calcite spherulite particles with fully spherical external morphologies showing internal fibro-radial and polycrystalline textures (Figures 2 and 3; Table S2). Spherulites appear as individual bodies (up to 30 μm in diameter) sparsely distributed on top of the frosted slides. In some cases, individual spherulites tend to aggregate horizontally until they form densely packed crusts (patches up to 300 μm in length) where spherical outlines can be difficult to clearly identify. Broken spherulites facilitate the observation of a fibro-radial crystalline internal fabric. The spherulite surfaces appear densely covered by an external coating of rhombic crystalline subunits (Figure 3C, D).

The deviation from the typical rhombohedral morphology of calcite can arise from the substantial Mg^{2+} ion contents in the synthetic lake water. In mineralising environments, an increased Mg^{2+}: Ca^{2+} ion ratio is known to transiently stabilise amorphous calcium carbonates (Loste et al., 2003; Radha et al., 2012). Following the non-classical pathways of crystallisation, the agglomeration and transformation of amorphous minerals can yield spherulite-like morphologies in Mg^{2+} rich environments (Cölfen and Antonieti, 2008; Huang et al., 2018). The radial crystalline internal fabric (Figure 3D) and surface textures also suggest the involvement of these particle accretion mechanisms, in which crystal growth occurs via the assembly and crystallisation of amorphous particles (De Yoreo et al., 2015; Rodríguez-Navarro et al., 2016).

3.2. Experiment 2: Low Salinity and with Organic Acids

Experiments performed with the identical salinity, but with the addition of 1 mg/L of alginic acid, produced calcite spherulite particles with smoother textures and coalesced forms (Figures 2 and 4; Table S2). Spherulites are present as individual bodies (up to 30 μm in diameter), but laterally linked spherulite habits are much more common and form densely horizontally accreted crusts (in patches up to 500 μm in length) or elongated and tightly packed spherulite aggregations with string-like morphologies (up to 600 μm in length; Figure 4C). Upward and outward aggregation of calcite spherulite bodies were consistently observed giving rise to shrubby tightly packed aggregates with prominent positive reliefs (Figure 4B, D). It is important to note that aggregation of polycrystalline spherulite bodies produces densely fused crystal solids rather than a simple cluster of spherules (Figure 4). These observations indicate the roles of acidic macromolecules in controlling not only mineral morphogenesis, but also early formative processes in nucleation and crystallisation.

Previous studies show that alginic acid can inhibit nucleation of mineral particles by sequestering Ca^{2+} ions and also, at elevated pH, by the stabilisation of Ca^{2+} and CO_3^{2-} ion clusters (Rao et al., 2016). Concurrently, the complexation of Ca^{2+} ions to the G units can lead to the self-association of alginate molecules following the 'egg-box' model (Fang et al., 2007). At the onset of particle nucleation, mineral precipitation can occur within the organo-metal matrix, i.e. the alginate-Ca^{2+}-CO_3^{2-} supramolecular assembly. Such mechanisms might yield aggregates of calcite spherulite bodies (Figure 4C, D). Moreover, the presence of localised mineral layers (Figure 4A) indicates the contributions of polymer-induced liquid-precursor (PILP) processes, in which liquid phase

mineral precursors are transiently stabilised by acidic macromolecules (Gower et al., 2000). Thus, in alkaline lake waters, solute state interactions between organic acids and mineral precursors can set the stage for the morphogenesis of aggregated and densely packed polycrystalline spherulites.

3.3. Experiment 3: High Salinity and without Organic Acids

Mineralisation experiments with salinities of 10.40 g/L NaCl and lacking organic acids produced spherulites showing internal fibro-radial and polycrystalline textures (Figures 2 and 5; Table S2). However, spherulite individual bodies (up to 15 μm in diameter) displayed both spherical and dumbbell-shaped morphologies. Bunches of well-defined calcite spherulites are seen forming granular clusters reaching up to 100 μm thick arborescent bodies with positive reliefs (Figure 5B). In this case, aggregation of polycrystalline spherulites produce loosely packed bodies rather than fused structures allowing individual spherules to be easily recognised (Figure 5). In addition, halite cubic single crystals (up to 50 μm in thickness) appeared intermingled between calcites (Figure 5D).

In comparison to the spherulites produced in low salinity experiments (Figure 3), high salinity environments appear to generate smaller particles, but not shrubby calcite. This emergence of smaller mineral particles at extreme salinity could be due to, first, faster nucleation rates on account of a decreased water-$CaCO_3$ interfacial energy with increasing ionic strength assuming the classical nucleation model (Li et al., 2019). However, it is also established that the pathways of $CaCO_3$ nucleation involve ion pairs, pre-nucleation clusters, liquid condensed phases and amorphous precursors (De Yoreo et al., 2015; Rodríguez-Navarro et al., 2016; Gebauer et al. 2018). In this respect, the occurrence of smaller particle size distributions is explained by the poor association of Ca^{2+} and CO_3^{2-} units prior to mineral nucleation at high salinity, for instance within pre-nucleation clusters and liquid condensed phases (Kellermeier et al. 2014. Here, high salinity conditions could support the existence of several minuscule, phase-separated nano-droplet precursors prior to mineral nucleation, thereby producing not only smaller mineral particles but also less rhombic surface coating (i.e. smoother textures) of the spherulites as morphological vestiges of the formative pathway.

3.4. Experiment 4: High Salinity and with Organic Acids

Mineralisation reactions in the presence of 10.40 g/L NaCl and 1 g/L of alginic acid produced subhedral to euhedral rhombic calcite crystals (up to 15 μm thick) showing smooth edges and, in some cases, displaying imbricated twin clusters up to 10 μm thick (Figures 2 and 6; Table S2). Calcites can be grouped in elongated strips hundreds of microns in length. Moreover, single crystals of cubic halite (up to 10 μm thick) were found imbricated between these carbonates. The total absence of upward growing arborescent habits is a common feature of these mineral assemblages (Figure 6).

An interesting observation is the formation of the thermodynamically favoured rhombohedral crystals of calcite at elevated salinity and alginic acid contents. From a mechanistic viewpoint, the influence of ionic strength alone on the solubility and conformation of alginic acid requires some consideration. For instance, the salting-out of alginic acid by increasing salt contents can deplete the macromolecular solutes (Rehm, 2009), which otherwise might interact with mineral precursors and regulate crystal growth. Here it is possible to show that the applied contents of background salts are critical in modulating the impacts of macromolecules on crystal formation. Increased salinity in the presence of alginic acid produces a switch from polycrystalline spherulite bodies (Figure 4) to euhedral morphologies (Figure 6). Furthermore, the presence of Mg^{2+} ions has previously been shown to mitigate the adsorption of alginic acids to carbonate surfaces (Browning et al., 2020). With the substantial effects of 'background' salts on the nucleation, growth and morphology of mineral particles (Burgos-Cara et al., 2017), chemical gradients associated with even simple monovalent ions might critically modulate the interactions between organic acid and mineral precursors and serve as a key determining factor for mineral form and structure in alkaline lake waters.

3.5. Hydrochemical considerations

Table S2 shows the hydrochemical data, average calcium, and magnesium consumption rates and mineralogies reported in experiments 1 to 4. A striking difference between the average calcium consumption in low saline (2.08 g/L of NaCl; experiments 1 and 2) and high saline (10.40 g/L of NaCl; experiments 3 and 4) reactions over 3 days is observed (Figure 7). While experiments 1 and 2 consumed about 99.76% and 99.66%, respectively, of the initial Ca^{2+} ion contents present in the flasks, experiments 3 and 4 exhausted 96.54% and 88.60%, respectively, of the net Ca^{2+} ions. Within this parameter space, high salinity appears to kinetically promote mineral nucleation, whereas the presence of alginic acid appears to inhibit mineral precipitation. Given that the pKa of

carboxylate groups in the sugar residues of alginate chains is about 3.5 (Donati and Paoletti, 2009), a fraction of Ca^{2+} ions sequestered by the carboxylate groups can affect the overall saturation. However, it is also important to consider the association of alginic acid with mineral precursors such as cluster species, liquid condensed phases and amorphous phases, which can produce an inhibitory activity towards mineral nucleation (Rao et al., 2016; Sebastiani et al., 2017). Experiments with organic acids appear to consume less Ca^{2+} ions than experiments without organics acids, with run 4 (high salinity and high alginic acid content) recording the minimum calcium depletion rates (Figure 7). Standard sample preparation for such chemical analyses involves filtration steps using sub-micron pores (typically 0.2 μm) which might have compromised the filtration efficiency of the alginic acid-ion complexes. As such, the estimated metal ion contents not only represent free ion species but also organic acid-bound metal ion species. The presence of (0.2 μm>) soluble organo-calcium complexes as well as the inhibitory effects of alginic acids towards mineral nucleation can explain the low fractions of Ca^{2+} ions consumed in alginic acid containing mineralisation reactions.

Indicative of the buffering effects of borate species, the pH changes during mineralisation are minor (increase from 12 to about 12.5) and the [Calcium]/[Alkalinity] ratios range between 0.134 and 0.138. All the experiments showed initial Mg/Si ratios of 9.061 and final values of 0 (Table S2). Moreover, saline experiments (1 and 2) recorded slightly lower initial SI calcite values (2.86) than the highly saline experiments 3 and 4 (2.96) estimated with PHREEQC.

3.6. Linking hydrochemistry with petrogenesis in Recent saline lakes and experiments

In view of the water compositions of saline lakes and laboratory experiments conducted in this work, four hydrochemical groups were identified on the basis of degree of salinity and [Calcium]/[Alkalinity] ratios (Groups 1 to 4 in Figure 8; Table 1). In natural settings, two main types of primary carbonate products have been documented: (i) biofilm-free sediments, normally formed as water column single-crystal micro-precipitates, and (ii) mounds or microbialites originated as benthic microbial accumulations made up of more diverse micro-crystal calcite assemblages (Figure 9; Table 1). The two-fold distinction is rather artificial as several constructive and destructive processes may have played in tandem leading to evolved forms (Ge et al., 2020). However, this classification is based on: i) micro-crystal precipitate morphology, and ii) location of authigenic precipitation (water column vs benthic).

Group 1. Low [Ca]/[Alk] ratios and low salinities. This group includes Mono Lake (USA) and Lake Van (Turkey), endorheic, saline lakes which are characterised by the highest alkalinity values (between 151 and 630 meq/L) and calcium concentrations between 0.074 and 0.514 meq/L (Figure 8; Table 1). The [Ca]/[Alk] ratios fluctuate between 4×10^{-4} and 1×10^{-3} while salinity values fall between 26 and 114 g/L. Loose carbonate particles consist of micron-sized calcite and aragonite flakes, and carbonaceous clayey silt. Carbonate microfabrics are represented by aragonite needles and dodecahedron-like calcite single crystals (Figure 9A, B) which resemble the micritic calcite precipitates found in other saline soda lakes from the USA Great Basin (Pyramid Lake, Figure 9C). Moreover, large microbialite chimneys are made up of homogenous clotted aragonitic to finely laminated low-Mg calcite microfabric and also groups of spheroidal bodies constituted by alternating dark and light concentric aragonitic to low-Mg calcite layers (Kempe et al., 1991; López-García et al., 2005).

Contemporaneous to Holocene Mono Lake carbonate sediments are dominated by a fine silt fraction of allochthonous tufa-rich sands and aragonite flake muds, representing about 7% of the total sediment volume in the first metres of the lake column (Newton, 1994). Furthermore, Mono Lake towers are constituted by an array of distinct microfabrics including leiolitic, clotted peloidal micrite, clotted microcolumnar and sinuous rims of micrite/ microsparite, the outermost Recent parts being mostly dominated by clotted peloidal micrite of microbial origin (Della Porta, 2015; Brasier et al., 2018).

Regarding the laboratory examples, the experiments by Tutolo and Tosca (2018) were designed with alkalinity and calcium concentrations broadly falling within the Mono Lake and Lake Van natural counterparts, with [Ca]/[Alk] values oscillating between 1×10^{-5} and 2×10^{-6}, and salinity values between 27 and 30 g/L. In general, these abiotic calcite precipitating runs produced an assemblage of dodecahedron-like, elongated dipyramid, protruded dipyramid and rhombic calcite single crystals (Figure 9D).

Group 2. Moderate [Ca]/[Alk] ratios and lower salinities. This group includes the experimental data presented here and the observations of Tracy et al. (1998a, b) regarding the growth of calcite spherulites from abiotic solutions. In both experimental datasets, alkalinity values are relatively high, between 14 and 131 meq/L and calcium concentrations between 17 and 100 meq/L. In addition, [Ca]/[Alk] ratios fluctuate between 0.138 and 2.72 while salinity values fall between 0.7 and 10.40 g/L (Figure 8; Table 1). In this group, calcite spherulite grains display a clear

polycrystalline, fibro-radial arrangement with grain diameters oscillating between 20 and 60 μm (Figure 9 E).

Group 3. Moderate [Ca]/[Alk] ratios and higher salinities. This hydrochemical group is represented by the Great Salt Lake: a hypersaline, endorheic lake. Alkalinity values are moderate, between 5.35 and 8.4 meq/L, and calcium concentrations are similar, between 6 and 16 meq/L. This enables [Ca]/[Alk] ratios to fluctuate between 0.9 and 3, while salinity concentrations show a remarkable variability between 84 and 490 g/L (Figure 8; Table 1). Contemporaneous Great Salt Lake sediments consist of muds, ooids, oncoids and bioherms/ microbial deposits (Chidsey et al., 2015; Della Porta, 2015; Vennin et al., 2018). Despite muds being volumetrically the most abundant sediment type, their calcium carbonate portion is thought to have been transported as wind or river particles to the lake (Eardley 1938; Bouton et al., 2019). The microfabrics of the carbonate bioherms/ microbialites consist of a leiolitic to clotted peloidal micrite/ microsparite hosting micritic laminae, peloids and coccoid components (Della Porta, 2015; Vennin et al., 2018). In addition, recently forming pustular microbial mats locally show a 'lumpy' or 'bumpy' texture composed of well-defined spherulitic calcite structures (Chidsey et al., 2015) (Figure 9F).

Group 4. Higher [Ca]/[Alk] ratios and moderate-high salinities. This group encompass the fresh to hypersaline Kiritimati atoll lakes (Central Pacific), hypersaline island lakes (Australia), and Lake Clifton coastal hyposaline lagoons (Australia). In this group, alkalinity values represent the lowest of the dataset, fluctuating between 1.71 and 4.25 meq/L, and having a range of calcium concentrations between 13.6 and 530 meq/L (Figure 8; Table 1). In addition, the resultant [Ca]/[Alk] ratios shift between 5.2 and 76.8, while salinity contents can vary between 16.8 and 373 g/L. Carbonate products documented in these natural settings include micrite muds, peloids, microbialite/ skeletal sands, thrombolite mounds and microbial mat-related spherulites (Figure 9G) to spherulitic microbialites (Figure 9I) (Burne and Moore, 1987; Moore, 1993; Burne et al., 2014; Arp et al., 2012; Bischoff et al., 2020).

In addition, experimental calcite precipitates falling within this hydrochemical group display alkalinity values of 37 meq/L, elevated calcium concentrations of 530 meq/L, [Ca]/[Alk] ratios of 14 and salinity concentrations of 53.8 g/L. In these batch experiments, the obtained polycrystalline calcite spherules reached 20 μm in diameter (Beck and Andreassen, 2010, their fig. 25).

4. DISCUSSION

4.1. Single-crystals vs Polycrystals: calcite crystal growth

This work shows that salinity, organic acid contents and alkalinity are key factors regulating the morphology and textural diversity of non-enzymatic carbonates as spherulites, agglomerates and rhombohedra. From the viewpoint of crystal growth, abiotic experiments with alkaline saline waters can precipitate abundant fibro-radial polycrystalline calcite spherulites. The elevated saturation indexes of the solutions (between 2.86 and 2.96), as well as the slow but gradual solvent evaporation are the driving forces for crystal formation and growth. Rather than the typical rhombohedral (equilibrium Wulff) form of calcite, spherulite morphologies are observed (experiments 1, 2 and 3). This morphogenesis is guided by the heterogeneous ionic compositions of the growth media, containing a Mg^{2+}: Ca^{2+} ratio of about 1 in these experiments. High Mg^{2+} ion contents can produce polycrystalline calcite particles even with simple fluid compositions (Reddy and Nancollas, 1976; Loste et al., 2003) and affect mineralisation pathways at distinct steps by (a) interacting with ion clusters (Wolf et al., 2015), and (b) regulating the water contents and stability of mineral precursors (Du et al., 2020; Huang et al., 2018). Further exploration of this parameter space will help generate a more robust correlation of the textural transitions of minerals in lake waters with complex fluid compositions and also elucidate the roles of chemical (inorganic and organic) gradients in petrographic diversity of calcites.

Considering the roles of salinity, an increase in NaCl contents produces smaller calcite spherulites with smoother textures. This is attributed to either lower water-$CaCO_3$ interfacial energies, which can yield several nucleation events with a short time span, or poor ion association at elevated salinity providing several mineral precursor droplets prior to nucleation. On the other hand, the introduction of alginic acids produces key modifications in crystal morphogenesis (Figure 10). Moderate contents of the organic acid (1 mg/L) lead to tightly packed spherulite aggregates. This organisation suggests that mineral precipitation occurs in association with an organic matrix rather than the post-mineralisation stacking of spherulites. This is also supported by the decreased solubility of alginates in the presence of Ca^{2+} and Mg^{2+} ions (Haud and Smidsrød, 1965). Thus, with moderate contents of the biopolymer, the nucleation and growth of mineral particles occurs within an organo-metal matrix (alginate-Ca^{2+}-CO_3^{2-} assembly), nonetheless retaining the effects of the (smaller) ionic species such as Mg^{2+} towards spherulite growth. With identical alginic acid contents but increased salinity (from 2.08g/L to 10.40g/L), the mineralisation reactions produce

prominent rhombohedral crystals of calcite (Figure 10A). This transition is attributed to the precipitation of alginic acids as calcium or magnesium salts under high salinity conditions (Haud and Smidsrød, 1965; Charfi et al., 2017). Such precipitation events deplete not only the organic acids but also divalent Ca^{2+} and Mg^{2+} ions from solution which otherwise mediate spherulite formation. In summary, in abiogenic waters, inorganic species such as Mg^{2+} affect mineral morphology and structure in a pH and salinity dependent manner. However, in the same environment, biopolymers affect mineralisation in a concentration dependent manner with indications of 'non-monotonicity'. Such 'non-monotonic' relationships between (i) net contents of ionic and organic molecules (additives) in mineralisation media and (ii) emergent crystal morphologies and structures arise from inter-additive interactions transpiring concurrent to mineral nucleation and growth. Such observations illustrate these complex relationships by identifying the dual roles of salinity on mineralisation in natural environments: first, in regulating the kinetics associated with nucleation, phase transformation and crystal growth and second, in modulating the availability (i.e. solubility) and depletion (i.e., precipitation) of ionic and organic species that regulate mineral morphogenesis.

4.2. Relationships between hydrochemistry and petrography in saline lacustrine carbonates

Sediments constituted by authigenic polycrystalline spherulites are remarkably rare in Recent saline lacustrine environments, where mud-size single crystals are volumetrically much more common. Some lacustrine evaporitic settings such as the Great Salt Lake, Kiritimati and Rottnest lagoons represent exquisite exceptions recording exotic Recent calcite spherulite sediments clearly occurring in association with microbial mat-related structures or their exopolymers in highly saline settings (Arp et al., 2012; Chidsey et al., 2015; Chafetz et al., 2018; Kirkham and Tucker, 2018; Bischoff et al., 2020).

Lake waters where Recent spherulite carbonates are formed (Groups 3 and 4) tend to have moderate to high [Ca]/[Alk] ratios (Figure 8; Table 1). Even though waters in Groups 3 and 4 are characterised by a range of saline to hypersaline values (between 16 and 490 g/L), spherulitic calcite all occurs as spherules rather than tightly packed vertically oriented shrubby aggregates such as those described in the Pre-Salt examples (Figure 1A, B; Gomes et al., 2020).

Group 2 shows a range of experimentally produced calcite spherulites and shrubby aggregates arising from solutions having moderate [Ca]/[Alk] ratios and remarkably low NaCl contents (between 0.7 and 10.40 g/L) (Figures 3, 4, 8 and 9E; Table 1). Thus, it seems that fluctuations in

salinity due to evaporation concentration (Great Salt Lake) or mixing with marine waters (Kiritimati or Rottnest lagoons) are not causatively related to the formation of calcite spherulites, or even the intermediate morphologies between spherulitic and shrubby calcite. The diameters of experimentally produced calcite spherulite clusters (up to 300 μm) and shrubby aggregates (up to 500 μm) are smaller than the allochems documented in the Pre-Salt assemblages or contemporaneous saline lakes (Figures 1A, B and 9). This probably reflects that the experiments contained a reduced mass of calcium and magnesium which was quickly consumed due to fast rates of calcite precipitation (Figure 7) limiting the dimensions of the particles. Therefore, size differences between Recent and ancient lake allochems and experimental grains are likely to respond to a scaling issue.

The abiotic experiments 1 and 3 described here allow the effects of small salinity variations in calcite morphology and precipitation rates to be examined (Figure 10A). In other words, it is possible to evaluate the impact that salinity fluctuations -likely occurring in evaporitic contexts- have on crystal shape. The [Ca]/[Alk] ratios in experiments 1 and 3 broadly fall within the ranges encouraging polycrystalline calcite in the preceding experiments (Tracy et al., 1998a, b). Also, slight salinity increments from 2.08 to 10.40 g/L in abiotic conditions did not encourage shrubby calcite, but rather reduced the size of the spherules from 30 to 15 μm (Figures 2, 3, 5 and 10A), and the calcite precipitation rate. The reduction in spherule size seems to run in parallel to the increase in salinity (ionic strength, Table S2) (experiment 3; Figure 7) which lowers the calcium removal rates of the solution.

Wider salinity values (between 16 and 490 g/L) recorded in lakes from Groups 3 and 4 (Figure 8, Table 1) do not seem to prevent the formation of spherulitic textures when they occur in association with microbial mats and their organic exopolymers (Chidsey et al., 2015; Arp et al., 2012; Bischoff et al., 2020). However, the observation that enhanced salinity and rising microbial organic contents (experiment 4 herein, Figure 10A) preclude the formation of synthetic polycrystalline calcite -actually promoting calcite single-crystals- disagrees with the observation of spherulites forming in saline and microbial-rich lakes of Groups 3 and 4 (Figures 9F, G, H and 10B).

This observation suggests that the inhibitory effect of increased salinity is likely offset by the potential biofilm metabolic effects increasing the pH and calcite saturation to promote spherulite calcification (Gallagher et al., 2010; Arp et al., 1999; 2012; Mercedes-Martín et al., 2017; Bischoff et al., 2020) (Figure 10B). Thus, despite bulk environmental perturbations, the presence of

biofilms or their biopolymers could have helped to maintain nearly constant SI values in the surrounding microbial ecospace facilitating biotically-influenced spherulite formation (*sensu* Bissett et al., 2008).

The combination of extremely low [Ca]/[Alk] ratios and higher alkalinities in Group 1 soda lakes is expected to preclude the abiotic formation of polycrystalline calcite in the lake waters as demonstrated by the type of sediments recognised in the first centimetres of Mono Lake beds (Newton, 1994), Lake Van (Stockhecke et al., 2014; McCormack et al., 2019) and Pyramid Lake (Arp et al., 1999; Reddy and Hoch, 2012) (Figure 9A, B, C). These authigenic sediments are dominated by micron-sized aragonitic muds showing single crystal rhombic to prismatic morphologies and considered as water column abiotic precipitates formed either as plume whitings in the river-lake mixing zone or due to evaporation-driven supersaturation processes (Reddy and Hoch, 2012; McCormack et al., 2019). Aragonite formation rather than calcite is preferred due to the high Mg/Ca in the lake water (Wang et al., 2012). Even though photosynthetic microbial activity can occur associated with Lake Van water column precipitates this process does not seem to promote spherulitic carbonate morphologies in such lake (see Figure 9A, B). This is because, in soda lakes, a minor rise in microbial photosynthesis-induced calcite supersaturation is observed because high alkalinity waters facilitate a large pH buffering (Arp et al., 1999; 2001), and the mineral formation rate will be limited by the very low [Ca]/[Alk] ratios (Wolters et al 2012) rendering the formation of calcite spherulites unlikely. A possible exception to this rule would occur in lake locations where calcium-rich groundwater mixes with alkaline lake waters locally increasing the [Ca]/[Alk] ratios of the mixture allowing an extra pumping of calcium enabling extreme calcite supersaturation and more equal [Ca]/[Alk] ratios (Figure 11A). Examples of calcium carbonate spherulitic grains forming in the mixing zones of alkaline soda lakes occur either in the lake shore of Pyramid Lake (Arp et al., 1999, page 171), or within Lake Van pinnacles (Kempe et al., 1991 page 607), and spring-feed tufa towers in Mono Lake (Figure 9H) (Della Porta, 2015). Remarkably in these examples, the formation of spherulitic microtextures occur in close spatial association with benthic microbial mats and their exopolymers rather than in the lake water column as purely abiotic precipitates (Brasier et al., 2019; Kempe et al., 1991). Consequently, the formation of lake floor spherulitic calcite allochems is likely to be very localised in soda lakes (Figure 11A).

The preference for waters with low [Ca]/[Alk] ratios and higher alkalinities (Group 1) to produce single crystal abiotic calcite has been also experimentally demonstrated by the formation of

dodecahedron-like and elongated to protruded dipyramid and rhombic calcite crystals (Tutolo and Tosca, 2018) (Figure 9D) resembling microcrystalline carbonates formed as abiotic whitings in the water column of Pyramid Lake (Arp et al., 1999) (compare Figure 9C with D). This suggests that calcite spherulites are more likely to occur in saline to hypersaline lake waters with moderate to high [Ca]/[Alk], low alkalinities, and aided by the counteracted effects of microbial metabolism and organic exopolymers (Figure 11B).

A notable exception to this rule seems to be the hyposaline Lake Clifton in Australia. Despite having high [Ca]/[Alk] and low alkalinity waters the thrombolitic deposits of this lake are characterised by the apparent absence of early formed carbonate phases including spherulitic carbonates (Burne et al., 2017).

5. CONCLUSIONS

By combining mineralogical and hydrochemical data from selected evaporitic lacustrine systems and lake water chemistry mimetic mineralisation experiments, the effects of salinity, calcium vs alkalinity, microbial metabolism, and organic acids in the formative processes of calcite spherulites and shrubby calcite have been explored. Spherulitic calcite preferentially forms in saline and/or alkaline waters in lacustrine and laboratory settings with a moderate to high [Ca]/[Alkalinity] ratio rather than in calcium-depleted systems (such as soda lakes). In addition, a causative relationship was not found between evaporative-driven salinity fluctuations (between 1 to 400 g/L of NaCl) and the preferential formation of either calcite spherulites, shrubs or their intermediate morphologies, bringing into question the role of evaporation alone towards spherulitic calcite development. Indeed, the experimental data suggests that salinity increments notably lowered the size of the calcite spherules and did not encourage shrubby calcite under the salinity range studied. This highlights the roles of concentration regimes associated with organic and inorganic molecules against the background salinity, conditioned by evaporation concentration, in determining the morphological and growth form transition of minerals. Spherulitic calcite growth did not occur in the presence of organic acids and high salinity implying that such inhibition is likely offset by the potential effects of microbial metabolic processes as recognised in all Recent spherulite-bearing lake systems. Consequently, microbial photosynthesis can raise the pH to levels allowing calcite supersaturation and spherulite mineralisation while organic molecules can impact the kinetics of spherulitic calcite aggregation in waters with moderate to high [Ca]/[Alkalinity] values.

Soda lake waters and experiments with low [Ca]/[Alkalinity] ratios and moderate salinity tend to produce an assemblage of single-crystal precipitates formed abiotically during water column mixing episodes or evaporation. Due to the calcium-limited nature of soda lake systems it is hypothesised that abiotic spherulitic calcite will be rather restricted in the lake water column (or sediment-water interface) as demonstrated by the type of micritic precipitates collected in Lake Van, Mono Lake or Pyramid Lake floors which formed abiotically in the water column. The unusual observation of spherulitic calcite components in Recent saline soda lakes (e.g., Mono Lake or Lake Van) can be explained by the existence of locally enhanced [Ca]/[Alkalinity] ratios occurring in specific lake locations where calcium-rich groundwaters mix with lake waters forming vertical chimneys on the lake floor. The close spatial association of microbial exopolymers with spherulites in these chimneys strongly advocates towards an organic acid control lowering the inhibitory effect of increased salinity, likely favouring spherulitic calcite nucleation.

ACKNOWLEDGEMENTS

Special thanks go to the scientists who generously contributed with their own photomicrograph and SEM material to illustrate the crystal assemblages discussed in this work. They include Gernot Arp, Karl Bischoff, Tom Chidsey, Giovanna Della Porta, João Gomes (under Petrobras permission), Jeremy McCormack, Sharon Tracy, and Benjamin Tutolo. Carlos Ayora is warmly thanked for stimulating discussions on Lake Chad geochemical modelling (Figure 1). We are grateful to the reviewers for critically reading and reviewing the manuscript, in particular the valuable comments and constructive and detailed criticism of Adrian Immenhauser and Nathan Rochelle-Bates. We also would like to thank Enrico Capezzuoli and Greta Swart for their Editorial assistance. MSR acknowledges financial support from Origin Center, project 190438131, Dutch Research Council (NWO) and Dutch National Science Agenda (NWA).

CONFLICT OF INTEREST

The authors declare that they have no known competing financial interests or personal relationships that could have appeared to influence the work reported in this paper.

DATA AVAILABILITY STATEMENT

The data for this study are shown in the various figures and in tables.

FIGURE CAPTIONS

Fig.1 A and B) Spherulitic carbonates recognised in Aptian Pre-Salt lacustrine settings. Fibro-radial polycrystalline calcite spherulites (white lines), and vertical and upward bifurcating, fascicular-optic to radial-fibrous, polycrystalline shrubs (yellow lines) coexisting with intermediate forms (red lines) (Courtesy J. Gomes, Petrobras). C) Previous thermodynamic model used to explain transitions between Pre-Salt minerals (green lines) as related to the water concentration factor in shallow evaporitic lakes (Wright and Tosca, 2016). Note that Na and Cl concentrations increase during evaporation. Despite CO_3 and Ca contents both initially increasing (stevensite zone), and CO_3 rising while Ca drops (calcite zone), the calcite solubility product remains broadly constant across the entire evaporative trajectory given that mineral precipitation is in equilibrium. D) Facies successions proposed for the Pre-Salt sediments as a result of increased evaporation (Wright and Barnett, 2015; Wright and Tosca, 2016).

Fig 2. A) Summary of the hydrochemical and petrographical data from experiments 1 to 4. B) X-ray powder diffraction data collected from Experiments 1 and 2. The lower set of lines indicates the expected peak positions and approximate intensities for a pure sample of calcite.

Fig. 3. Calcite precipitates from Experiment 1 (Alginic acid: 0 mg/L, NaCl: 2.08 g/L). A) Generalised view of the frosted slide covered by calcite spherules. B) Clusters of polycrystalline calcite spherulites aggregating horizontally. C) The external outlines of the spherulites are densely covered by a coating of calcite rhombs. D) Broken spherulites facilitate the observation of a fibro-radial crystalline internal texture (arrows). Yellow asterisks indicate EDS spot analysis measurement points.

Fig. 4. Calcite precipitates from Experiment 2 (Alginic acid: 1 mg/L, NaCl: 2.08g/L). A) Calcite coverage is localised in specific areas of the frosted slides showing distinct upward and outward aggregation (arrows). B) Calcite spherulite bodies give rise to shrubby tightly packed aggregates with prominent positive reliefs (arrows). C) Detail of tightly packed spherulite aggregations

forming string-like structures. D) Lateral view showing aggregation of polycrystalline spherulite bodies producing densely fused, upwards growing crystal solids (arrows). Yellow asterisks indicate EDS spot analysis measurement points.

Fig. 5. Calcite precipitates from Experiment 3 (Alginic acid: 0 mg/L, NaCl: 10.40g/L). A) Generalised view showing a reduction of calcite spherulite slide coverage and diameters. B) Calcite forming granular, arborescent clusters of loosely packed spherulitic bodies (arrows). C) Both spherical and dumbbell-shaped calcite spherulites coexist (arrow). D) Halite cubic single crystals are common intermingled between calcite crystals (arrows). Yellow asterisks indicate EDS spot analysis measurement points.

Fig. 6. Calcite precipitates from Experiment 4 (Alginic acid: 1 mg/L, NaCl: 10.40 g/L). A) Generalised view of tiny rhombic euhedral calcite crystals covering the slides in elongated strips. B) Rhombic crystals (up to 15 μm thick) showing smooth edges. C) Detail of rhombic crystals showing imbricated twin clusters. D) Detail of imbricated twin clusters in C (arrows). Yellow asterisks indicate EDS spot analysis measurement points.

Fig. 7. Calcium concentration in solutions (n=4) after experiment termination. A) Low salinity experiment (2.08 g/L NaCl). B) High salinity experiment (10.40 g/L NaCl).

Fig. 8. Hydrochemical data from saline lacustrine settings and experiments examined in this work. Logarithmic plot of Salinity vs Calcium/ Alkalinity showing the hydrochemical categories in this work (Groups 1 to 4). See legend and Table 1 for more details.

Fig. 9. SEM and thin-section photomicrographs of calcite petrographies from natural lacustrine sites and experiments from Groups 1 to 4. A and B) Carbonate microfabrics represented by aragonite dodecahedron-like calcite single crystals (dod), and prismatic aggregated needles (pris) formed in the water column of Lake Van (Courtesy J. McCormack). C) Water column micritic calcite precipitates showing dodecahedron-like calcite single crystal morphologies (dod) in Pyramid Lake, USA (Courtesy G. Arp). D) An assemblage of protruded dipyramid (dip) and rhombic calcite single crystals (rho) formed in abiotic experimental runs (Courtesy B. Tutolo). E) Calcite spherulites with fibro-radial growths (arrows) from experimental runs (left) (from Tracy et

al., 1998a). Note that fibres (arrows) are densely covered by a coating of single rhombic calcite crystals (right image) (Courtesy S. Tracy). F) Great Salt Lake (USA) Recent pustular microbial mats locally show a 'lumpy' texture composed of spherulitic calcite structures formed in the lake mixing zone (arrows) (Courtesy T. Chidsey). G) Microbial mat-related spherulites growing in hypersaline to fresh lagoons in Kiritimati (Central Pacific) (Courtesy G. Arp). H) Clotted peloidal micrite and sinuous threads forming subspherical structures of micrite to fibrous crystal cementstone (arrows) from Mono Lake spring pinnacles (Courtesy G. Della Porta). I) Cluster of calcite spherulites formed in association with microbial communities (microbialites) at Rottnest hypersaline lagoons (Australia) (Courtesy K. Bischoff).

Fig. 10. A) Summary of hydrochemical conditions giving rise to calcite petrographical features from experiments 1 to 4 herein. Polycrystalline and upward growing calcite aggregates can be better explained where abundant alginic acid concentrations coexist with high [Calcium]/[Alkalinity] waters (acronym: [Ca/Alk]). See Figure 2 for details. B) Conceptual scheme illustrating the hydrochemical groups according to [Ca/Alk] ratios and salinities. Red double-arrowed lines refer to likely routes between hydrochemical groups 2 to 4 in which calcite spherulite formation has been commonly recognised. The black arrow represents mixing of calcium-rich groundwaters (Group 2) with soda lake waters (Group 1) producing enhanced [Ca/Alk] waters that can lead to localised formation of calcite spherulites.

Fig. 11. A and B) Depositional models for Group 1 and Groups 3 and 4 lakes, respectively, summarising the overall processes and carbonate precipitates (water column, loose particles, and microbial benthic structures). The colour pattern links processes with carbonate products.

Table 1. Summary of the hydrochemical and petrographical data from the studied saline, alkaline lakes, and experimental datasets (including experiments herein). Source list on the right refers to petrographic data from naturally occurring sites.

Table S1. Summary of the batch solutions for experiments. Low salinity (experiments 1 and 2) and high salinity (experiments 3 and 4).

Table S2. Hydrochemical data from experiments. Notation (i) and (f) indicate values recorded at the beginning and the end of the experiments, respectively.

REFERENCES

Addadi, L., Raz, S., and Weiner, S. (2003). Taking advantage of disorder: Amorphous calcium carbonate and its roles in biomineralization. *Advanced Materials*, 15(12), 959–970. https://doi.org/10.1002/adma.200300381

Arp, G., Helms, G., Karlinska, K., Schumann, G., Reimer, A., Reitner, J., and Trichet, J. (2012). Photosynthesis versus exopolymer degradation in the formation of microbialites on the atoll of Kiritimati, Republic of Kiribati, Central Pacific. *Geomicrobiology Journal*, *29*(1), 29-65.

Arp, G., Thiel, V., Reimer, A., Michaelis, W., and Reitner, J. (1999). Biofilm exopolymers control microbialite formation at thermal springs discharging into the alkaline Pyramid Lake, Nevada, USA. *Sedimentary Geology*, *126*(1-4), 159-176.

Beck, R., and Andreassen, J. P. (2010). Spherulitic growth of calcium carbonate. *Crystal Growth & Design*, *10*(7), 2934-2947.

Bischoff, K., Sirantoine, E., Wilson, M. E., George, A. D., Mendes Monteiro, J., and Saunders, M. (2020). Spherulitic microbialites from modern hypersaline lakes, Rottnest Island, Western Australia. *Geobiology*. https://doi.org/10.1111/gbi.12400

Bissett, A., Reimer, A., de Beer, D., Shiraishi, F., and Arp, G. (2008). Metabolic microenvironmental control by photosynthetic biofilms under changing macroenvironmental temperature and pH conditions. *Applied and Environmental Microbiology*, 74(20), 6306-6312.

Bosak, T., Souza-Egipsy, V., and Newman, D. K. (2004). A laboratory model of abiotic peloid formation. *Geobiology*, *2*(3), 189-198.

Bouton, A., Vennin, E., Amiotte-Suchet, P., Thomazo, C., Sizun, J. P., Virgone, A., and Visscher, P. T. (2019). Prediction of the calcium carbonate budget in a sedimentary basin: A "source-to-sink" approach applied to Great Salt Lake, Utah, USA. *Basin Research*.

Brasier, A. T., Rogerson, M. R., Mercedes-Martin, R., Vonhof, H. B., and Reijmer, J. J. G. (2015). A test of the biogenicity criteria established for microfossils and stromatolites on Quaternary tufa and speleothem materials formed in the "Twilight Zone" at Caerwys, UK. *Astrobiology*, *15*(10), 883-900.

Browning, K. L., Stocker, I. N., Gutfreund, P., & Clarke, S. M. (2020). The effect of alginate composition on adsorption to calcium carbonate surfaces. *Journal of Colloid and Interface Science.*

Burgos-Cara, A., Putnis, C. V., Rodriguez-Navarro, C., and Ruiz-Agudo, E. (2017). Hydration effects on the stability of calcium carbonate pre-nucleation species. *Minerals*, 7(7), 126.

Burne, R. V., and Moore, L. S. (1987). Microbialites; organosedimentary deposits of benthic microbial communities. *Palaios*, *2*(3), 241-254.

Burne, R. V., Moore, L. S., Christy, A. G., Troitzsch, U., King, P. L., Carnerup, A. M., and Hamilton, P. J. (2014). Stevensite in the modern thrombolites of Lake Clifton, Western Australia: A missing link in microbialite mineralization? *Geology*, *42*(7), 575-578.

Capezzuoli, E., Gandin, A., and Pedley, M. (2014). Decoding tufa and travertine (freshwater carbonates) in the sedimentary record: The state of the art. *Sedimentology*, 61(1), 1-21.

Chafetz, H., Barth, J., Cook, M., Guo, X., and Zhou, J. (2018). Origins of carbonate spherulites: implications for Brazilian Aptian pre-salt reservoir. *Sedimentary Geology*, *365*, 21-33.

Chan, M. A., Hinman, N. W., Potter-McIntyre, S. L., Schubert, K. E., Gillams, R. J., Awramik, S. M., and Jia, T. Z. (2019). Deciphering biosignatures in planetary contexts. *Astrobiology*, 19(9), 1075-1102.

Charfi, A., Jang, H., and Kim, J. (2017). Membrane fouling by sodium alginate in high salinity conditions to simulate biofouling during seawater desalination. *Bioresource technology*, 240, 106-114.

Chidsey, T. C., Berg, M. D. V., and Eby, D. E. (2015). Petrography and characterization of microbial carbonates and associated facies from modern Great Salt Lake and Uinta Basin's Eocene Green River Formation in Utah, USA. *Geological Society, London, Special Publications*, *418*(1), 261-286.

Cölfen, H., and Antonietti, M. (2008). Mesocrystals and nonclassical crystallization. John Wiley & Sons.

Connell, T. L., and Dreiss, S. J. (1995). Chemical evolution of shallow groundwater along the northeast shore of Mono Lake, California. *Water Resources Research*, *31*(12), 3171-3182.

Darragi, F., and Tardy, Y. (1987). Authigenic trioctahedral smectites controlling pH, alkalinity, silica and magnesium concentrations in alkaline lakes. *Chemical Geology*, *63*(1-2), 59-72.

Della Porta, G. (2015). Carbonate build-ups in lacustrine, hydrothermal and fluvial settings: comparing depositional geometry, fabric types and geochemical signature. *Geological Society, London, Special Publications*, *418*(1), 17-68.

Deocampo, D. M., and Renaut, R. W. (2016). Geochemistry of African soda lakes. In *Soda Lakes of East Africa* (pp. 77-93). Springer, Cham.

De Yoreo, J. J., Gilbert, P. U., Sommerdijk, N. A., Penn, R. L., Whitelam, S., Joester, D., and Wallace, A. F. (2015). Crystallization by particle attachment in synthetic, biogenic, and geologic environments. *Science*, 349(6247).

Donati, I., and Paoletti, S. (2009). Material properties of alginates. In Alginates: Biology and applications (pp. 1-53). Springer, Berlin, Heidelberg.

Du, H., Courrégelongue, C., Xto, J., Böhlen, A., Steinacher, M., Borca, C. N., and Amstad, E. (2020). Additives: their influence on the humidity-and pressure-induced crystallization of amorphous CaCO3. *Chemistry of Materials*, 32(10), 4282-4291.

Eardley, A. J. (1938). Sediments of Great Salt Lake, Utah. *AAPG Bulletin*, 22 (10), 1305–1411.

Erthal, M. M., Capezzuoli, E., Mancini, A., Claes, H., Soete, J., and Swennen, R. (2017). Shrub morpho-types as indicator for the water flow energy-Tivoli travertine case (Central Italy). *Sedimentary Geology*, 347, 79-99.

Eugster, H. P., and Hardie, L. A. (1978). Saline lakes. In *Lakes* (pp. 237-293). Springer, New York, NY.

Fang, Y., Al-Assaf, S., Phillips, G. O., Nishinari, K., Funami, T., Williams, P. A., and Li, L. (2007). Multiple steps and critical behaviors of the binding of calcium to alginate. The *Journal of Physical Chemistry* B, 111(10), 2456-2462.

Farias, F., Szatmari, P., Bahnieuk, A., and Barros França, A., 2019. Evaporitic carbonates in the pre-salt of Santos Basin – Genesis and tectonic implications. *Marine and Petroleum Geology*, 105, 251-272.

Fouke, B.W., 2011. Hot-spring Systems Geobiology : abiotic and biotic influences on travertine formation at Mammoth Hot Springs, Yellowstone National Park , USA. *Sedimentology*, 58, (1). 170–219.

Frisia, S., Borsato, A., Fairchild, I.J. and McDermott, F. (2000). Calcite Fabrics, Growth Mechanisms, and Environments of Formation in Speleothems from the Italian Alps and Southwestern Ireland. *Journal of Sedimentary Research* 70(5), 1183-1196.

Gallagher, K., Dupraz, C., Braissant, O., Norman, R., Decho, A., and Visscher, P. T. (2010). Mineralization of sedimentary biofilms: modern mechanistic insights. Biofilm: Formation, *Development and Properties. Nova Science Publishers*.

Ge, Y., Lokier, S. W., Hoffmann, R., Pederson, C. L., Neuser, R. D., and Immenhauser, A. (2020). Composite micrite envelopes in the lagoon of Abu Dhabi and their application for the recognition of ancient firm-to hardgrounds. *Marine Geology*, 423, 106141.

Gebauer, D (2018). How can additives control the early stages of mineralisation? *Minerals* 8.5: 179

Gomes, J. P., Bunevich, R. B., Tedeschi, L. R., Tucker, M. E., and Whitaker, F. F. (2020). Facies classification and patterns of lacustrine carbonate deposition of the Barra Velha Formation, Santos Basin, Brazilian Pre-salt. *Marine and Petroleum Geology*, 113, 104176.

Gower, L. B., and Odom, D. J. (2000). Deposition of calcium carbonate films by a polymer-induced liquid-precursor (PILP) process. *Journal of Crystal Growth*, 210(4), 719-734.

Haug, A., and Smidsrød, O. (1965). Fractionation of alginates by precipitation with calcium and magnesium ions. *Acta Chem. Scand*, 19(5).

Herlinger, R., Zambonato, E.E., and Ros, L.F.D.E., (2017). Influence of Diagenesis on the Quality of Lower Cretaceous Pre-Salt Lacustrine Carbonate Reservoirs From Northern Campos Basin, Offshore Brazil. *Journal of Sedimentary Research*, 1285–1313.

Hodgson, D. M., Bernhardt, A., Clare, M., A., Da Silva, A-C., Fosdick, J. C., Mauz, B., Midtkandal, I., Owen, A., and Romans, B. W. (2018). Grand Challenges (and Great Opportunities) in Sedimentology, Stratigraphy, and Diagenesis Research. *Frontiers in Earth Sciences*, 23. https://doi.org/10.3389/feart.2018.00173

Huang, Y. C., Gindele, M. B., Knaus, J., Rao, A., and Gebauer, D. (2018). On mechanisms of mesocrystal formation: magnesium ions and water environments regulate the crystallization of amorphous minerals. *CrystEngComm*, 20(31), 4395-4405

Imai, H., (2016). Mesostructured crystals: Growth processes and features. *Progress in Crystal Growth and Characterization of Materials*, 62 (2), 212-226.

Irion G (1973) Die anatolischen Salzseen, ihr Chemismus und die Entstehung ihrer chemischen Sedimente. *Arch Hydrobiol* 71:517–557

Jones, B. (1994). Diagenetic processes associated with plant roots and microorganisms in karst terrains of the Cayman Islands, British West Indies. *Developments in Sedimentology*, 51, 425-475.

Jones, B. (2017). Review of aragonite and calcite crystal morphogenesis in thermal spring systems. *Sedimentary Geology*, 354, 9-23.

Jones, B. F. (1986). Clay mineral diagenesis in lacustrine sediments. *Studies in diagenesis*, *1578*, 291-300.

Jones, B., and Peng, X. (2014). Signatures of biologically influenced CaCO3 and Mg–Fe silicate precipitation in hot springs: Case study from the Ruidian geothermal area, western Yunnan Province, China. *Sedimentology*, 61(1), 56-89.

Jones, B., and Renaut, R. W. (1995). Noncrystallographic calcite dendrites from hot-spring deposits at Lake Bogoria, Kenya. *Journal of Sedimentary Research*, 65(1).

Kelts, K., and Talbot, M. (1990). Lacustrine carbonates as geochemical archives of environmental change and biotic/abiotic interactions. In *Large Lakes* (pp. 288-315). Springer, Berlin, Heidelberg.

Kellermeier, M., Picker, A., Kempter, A., Cölfen, H., and Gebauer, D. (2014). A straightforward treatment of activity in aqueous CaCO3 solutions and the consequences for nucleation theory. *Advanced Materials*, 26(5), 752-757.

Kempe, S., Kazmierczak, J., Landmann, G., Konuk, T., Reimer, A., and Lipp, A. (1991). Largest known microbialites discovered in Lake Van, Turkey. *Nature*, *349*(6310), 605-608.

Kirkham, A., and Tucker, M. E. (2018). Thrombolites, spherulites and fibrous crusts (Holkerian, Purbeckian, Aptian): Context, fabrics and origins. *Sedimentary Geology*, *374*, 69-84.

Li, Q., & Jun, Y. S. (2019). Salinity-Induced Reduction of Interfacial Energies and Kinetic Factors during Calcium Carbonate Nucleation on Quartz. *The Journal of Physical Chemistry* C, 123(23), 14319-14326.

Lima, B. E. M., and De Ros, L. F. (2019). Deposition, diagenetic and hydrothermal processes in the Aptian Pre-Salt lacustrine carbonate reservoirs of the northern Campos Basin, offshore Brazil. *Sedimentary Geology*, *383*, 55-81.

López-García, P., Kazmierczak, J., Benzerara, K., Kempe, S., Guyot, F., and Moreira, D. (2005). Bacterial diversity and carbonate precipitation in the giant microbialites from the highly alkaline Lake Van, Turkey. *Extremophiles*, *9*(4), 263-274.

Loste, E., Wilson, R. M., Seshadri, R., and Meldrum, F. C. (2003). The role of magnesium in stabilising amorphous calcium carbonate and controlling calcite morphologies. *Journal of Crystal Growth*, 254(1-2), 206-218

Luiz-Dias, J. (2005). Tectônica, estratigrafia e sedimentação no Andar Aptiano da margem leste brasileira. Boletim Geociencias Petrobras, 13, 1, 7-25.

Ma, Y., and Feng, Q. (2015). A crucial process: Organic matrix and magnesium ion control of amorphous calcium carbonate crystallization on ??-chitin film. *CrystEngComm*, 17(1), 32–39. https://doi.org/10.1039/c4ce01616e

McCormack, J., Nehrke, G., Jöns, N., Immenhauser, A., and Kwiecien, O. (2019). Refining the interpretation of lacustrine carbonate isotope records: Implications of a mineralogy-specific Lake Van case study. *Chemical Geology*, *513*, 167-183.

McLoughlin, N., Brasier, M. D., Wacey, D., Green, O. R., and Perry, R. S. (2007). On biogenicity criteria for endolithic microborings on early Earth and beyond. *Astrobiology*, *7*(1), 10-26.

Meldrum, F. C., and Cölfen, H. (2008). Controlling mineral morphologies and structures in biological and synthetic systems. *Chemical Reviews*, *108*(11), 4332-4432.

Mercedes-Martín, R., Brasier, A. T., Rogerson, M., Reijmer, J. J., Vonhof, H., and Pedley, M. (2017). A depositional model for spherulitic carbonates associated with alkaline, volcanic lakes. *Marine and Petroleum Geology*, *86*, 168-191.

Mercedes-Martín, R., Rogerson, M. R., Brasier, A. T., Vonhof, H. B., Prior, T. J., Fellows, S. M., and Pedley, H. M. (2016). Growing spherulitic calcite grains in saline, hyperalkaline lakes: experimental evaluation of the effects of Mg-clays and organic acids. *Sedimentary Geology*, *335*, 93-102.

Mercedes-Martín, R., Ayora, C., Tritlla, J., & Sánchez-Román, M. (2019). The hydrochemical evolution of alkaline volcanic lakes: a model to understand the South Atlantic Pre-salt mineral assemblages. *Earth-Science Reviews*, 198, 102938.

Moore, L. S. (1987). Water chemistry of the coastal saline lakes of the Clifton-Preston Lakeland System, south-western Australia, and its influence on stromatolite formation. *Marine and Freshwater Research*, 38(5), 647-660.

Moore, L. (1993). The modern microbialites of Lake Clifton, south-western Australia. University of Western Australia, Perth.

Morse, J. W., Arvidson, R. S., and Lüttge, A. (2007). Calcium carbonate formation and dissolution. *Chemical Reviews*, *107* (2), 342-381.

Muniz, M. C., and Bosence, D. W. J. (2015). Pre-salt microbialites from the Campos Basin (offshore Brazil): image log facies, facies model and cyclicity in lacustrine carbonates. *Geological Society, London, Special Publications*, *418*(1), 221-242.

Newton, M. S. (1994). Holocene fluctuations of Mono Lake, California: the sedimentary record. Sedimentology and Geochemistry of Modern and Ancient Saline Lakes, *SEPM Special Publication*, 50, 143-157.

Parkhurst, D. L., and Appelo, C. A. J. (2013). Description of input and examples for PHREEQC version 3: a computer program for speciation, batch-reaction, one-dimensional transport, and inverse geochemical calculations (No. 6-A43). *US Geological Survey*.

Pedley, H.M., Rogerson, M. and Middleton, R. (2009). The growth and morphology of freshwater calcite precipitates from in vitro mesocosm flume experiments; the case for biomediation. *Sedimentology* 56, 511-527.

Radha, A. V., Fernandez-Martinez, A., Hu, Y., Jun, Y. S., Waychunas, G. A., and Navrotsky, A. (2012). Energetic and structural studies of amorphous Ca1− xMgxCO3· nH2O (0⩽ x⩽ 1). *Geochimica et Cosmochimica Acta*, 90, 83-95.

Rainey, D. K., and Jones, B. (2009). Abiotic versus biotic controls on the development of the Fairmont Hot Springs carbonate deposit, British Columbia, Canada. *Sedimentology*, 56(6), 1832-1857.

Rao, A., Vásquez-Quitral, P., Fernández, M. S., Berg, J. K., Sánchez, M., Drechsler, M., and Cölfen, H. (2016). pH-dependent schemes of calcium carbonate formation in the presence of alginates. *Crystal Growth & Design*, 16(3), 1349-1359.

Reddy, M. M., and Hoch, A. (2012). Calcium carbonate nucleation in an alkaline lake surface water, Pyramid Lake, Nevada, USA. *Aquatic geochemistry*, *18*(2), 95-113.

Reddy, M. M., and Nancollas, G. H. (1976). The crystallization of calcium carbonate: IV. The effect of magnesium, strontium and sulfate ions. *Journal of Crystal Growth*, 35(1), 33-38.

Rehm, B. H. (Ed.). (2009). Alginates: biology and applications (Vol. 13). Springer Science & Business Media.

Reimer, A., Landmann, G., and Kempe, S. (2009). Lake Van, eastern Anatolia, hydrochemistry and history. *Aquatic Geochemistry*, 15(1-2), 195-222.

Rodriguez-Navarro, C., Burgos Cara, A., Elert, K., Putnis, C. V., & Ruiz-Agudo, E. (2016). Direct nanoscale imaging reveals the growth of calcite crystals via amorphous nanoparticles. *Crystal Growth & Design*, 16(4), 1850-1860.

Rogerson, M., Mercedes-Martín, R., Brasier, A. T., McGill, R. A., Prior, T. J., Vonhof, H., Fellows, S. M., Reijmer, J. J. G., McClymont, E., Billing, I., Matthews, A., and Pedley, M. (2017). Are spherulitic lacustrine carbonates an expression of large-scale mineral carbonation? A case study from the East Kirkton Limestone, Scotland. *Gondwana Research,* 48, 101-109.

Saller, A., Rushton, S., Buambua, L., Inman, K., McNeil, R., and Dickson, J. T. (2016). Presalt stratigraphy and depositional systems in the Kwanza Basin, offshore Angola. *AAPG Bulletin*, 100(7), 1135-1164.

Sánchez-Navas, A., Martin-Algarra, A., Sánchez-Roman, M., Jiménez-López, C., Nieto, F., and Ruiz-Bustos, A. (2013). Crystal growth of inorganic and biomediated carbonates and phosphates. *Advanced Topics on Crystal Growth*. pp. 1-22.

Sánchez-Román M, Vasconcelos C, Schmidt T, Dittrich M, McKenzie JA, Zenobi R, and Rivadeneyra, M.A. (2008). Aerobic microbial dolomite at the nanometer scale: Implications for the geologic record. *Geology* 36, 879-882.

Sánchez-Román M, Vasconcelos C, Warthmann R, Rivadeneyra MA. and McKenzie, J.A. (2009) Microbial Dolomite Precipitation under Aerobic Conditions: Results from Brejo do Espinho Lagoon (Brazil) and Culture Experiments. In: Perspectives in Carbonate Geology: A Tribute to the Career of Robert Nathan Ginsburg (eds P. K. Swart, G. P. Eberli, J. A. McKenzie, I. Jarvis and T. Stevens). *Sedimentology* (IAS Spec Publ No. 40), p. 167- 178.

Sánchez-Román M, McKenzie JA, de Luca Rebello Wagener A, Romanek CS, Sánchez-Navas A, and Vasconcelos C. (2011). Experimentally determined biomediated Sr^{2+} partition coefficient for dolomite: Significance and implication for natural dolomite. *Geochimica et Cosmochimica Acta* 75, 887-904.

Sanz-Montero E, Cabestrero O, Sánchez-Román M (2019) Microbially mediated Mg-rich carbonates in extreme alkaline lakes. *Frontiers in Microbiology* 10, 148.

Sebastiani, F., Wolf, S. L., Born, B., Luong, T. Q., Cölfen, H., Gebauer, D., and Havenith, M. (2017). Water dynamics from THz spectroscopy reveal the locus of a liquid–liquid binodal limit in aqueous CaCO3 solutions. *Angewandte Chemie International Edition*, 56(2), 490-495.

Schweizer G (1975) Untersuchungen zur Physiogeographie von Ostanatolien und Nordwestiran, geomor- phologische, klima- und hydrogeographische Studien im Vansee- und Rezaiyehsee-Gebiet. Tu¨binger Geogr Studien 60:145 pp, Selbstverl. Geogr Inst Univ Tubingen.

Serebryakov, S. N. (1976). Biotic and abiotic factors controlling the morphology of Riphean stromatolites. In *Developments in Sedimentology* (Vol. 20, pp. 321-336). Elsevier.

Stalport, F., Coll, P., Cabane, M., Person, A., González, R. N., Raulin, F., and Zarnecki, J. (2005). Search for past life on Mars: Physical and chemical characterization of minerals of biotic and abiotic origin: Part 1-calcite. *Geophysical research letters*, *32*(23).

Stockhecke, M., Kwiecien, O., Vigliotti, L., Anselmetti, F. S., Beer, J., Çağatay, M. N., and Pickarski, N. (2014). Chronostratigraphy of the 600,000-year-old continental record of Lake Van (Turkey). *Quaternary Science Reviews*, *104*, 8-17.

Taylor, P. M., and Chafetz, H. S. (2004). Floating rafts of calcite crystals in cave pools, central Texas, USA: crystal habit vs. saturation state. *Journal of Sedimentary Research*, *74*(3), 328-341.

Terra et al., (2010). Classificação de rochas carbonáticas aplicável às bacias sedimentares brasileiras. *Bulletin Geoscience Petrobras, Rio de Janeiro*, 18 (1), 9-29.

Tosca, N. J., and Masterson, A. L. (2014). Chemical controls on incipient Mg-silicate crystallization at 25 C: Implications for early and late diagenesis. *Clay Minerals*, *49*(2), 165-194.

Tosca, N. J., and Wright, V. P. (2015). Diagenetic pathways linked to labile Mg-clays in lacustrine carbonate reservoirs: a model for the origin of secondary porosity in the Cretaceous pre-salt Barra Velha Formation, offshore Brazil. *Geological Society, London, Special Publications*, *435*(1), 33-46.

Tracy, S. L., François, C. J. P., and Jennings, H. M. (1998a). The growth of calcite spherulites from solution: I. Experimental design techniques. *Journal of crystal growth*, *193*(3), 374-381.

Tracy, S. L., Williams, D. A., and Jennings, H. M. (1998b). The growth of calcite spherulites from solution: II. Kinetics of formation. *Journal of Crystal Growth*, *193*(3), 382-388.

Tutolo, B. M., and Tosca, N. J. (2018). Experimental examination of the Mg-silicate-carbonate system at ambient temperature: Implications for alkaline chemical sedimentation and lacustrine carbonate formation. *Geochimica et Cosmochimica Acta*, *225*, 80-101.

Vennin, E., Bouton, A., Bourillot, R., Pace, A., Roche, A., Brayard, A., and Visscher, P. T. (2019). The lacustrine microbial carbonate factory of the successive Lake Bonneville and Great Salt Lake, Utah, USA. *Sedimentology*, *66*(1), 165-204.

Wacey, D. (2010). Stromatolites in the ~3400 Ma Strelley Pool Formation, Western Australia: examining biogenicity from the macro-to the nano-scale. *Astrobiology*, *10*(4), 381-395.

Wang, D., Hamm, L. M., Giuffre, A. J., Echigo, T., Rimstidt, J. D., De Yoreo, J. J., and Dove, P. M. (2012). Revisiting geochemical controls on patterns of carbonate deposition through the lens of multiple pathways to mineralization. *Faraday Discussions*, 159(1), 371-386.

Webb, G. E. (1996). Was Phanerozoic reef history controlled by the distribution of non-enzymatically secreted reef carbonates (microbial carbonate and biologically induced cement)? *Sedimentology*, *43*(6), 947-971.

Wilkinson, B. H., and Given, R. K. (1986). Secular variation in abiotic marine carbonates: constraints on Phanerozoic atmospheric carbon dioxide contents and oceanic Mg/Ca ratios. *The Journal of Geology*, *94*(3), 321-333.

Wolf, S. L., Jähme, K., and Gebauer, D. (2015). Synergy of Mg 2+ and poly (aspartic acid) in additive-controlled calcium carbonate precipitation. *CrystEngComm*, 17(36), 6857-6862.

Wolthers, M., Nehrke, G., Gustafsson, J. P., & Van Cappellen, P. (2012). Calcite growth kinetics: Modeling the effect of solution stoichiometry. *Geochimica et Cosmochimica Acta*, 77, 121-134.

Wright, P., and Tosca, N. (2016). A Geochemical Model for the Formation of the Pre-Salt Reservoirs, Santos Basin, Brazil: Implications for Understanding Reservoir Distribution. In *AAPG Annual Convention and Exhibition*.

Wright, V.P. (2012). Lacustrine carbonates in rift settings: the interaction of volcanic and microbial processes on carbonate deposition. *Geol. Soc. London, Spec. Publ*. 39–47. https://doi.org/10.1144/SP370.2

Case study	Reference	Region	Sample source	Hydrological features	pH	Salinity	Alkalinity	Ca	Mg	Mg/Ca	Ca/ Alk	Ca+Mg/ Alk	Hydrochemical group	Summary carbonate products		References
						g/L	meq/L	meq/L	meq/L					Sediments	Benthic microbial textures/ deposits	
Lake Van	Reimer et al.,2009	Eastern Anatolia, (Turkey)	5m depth (1989)	Endorheic, saline, alkaline lake	9.73	27.43	151	0.210	8.80	42.0	0.001	0.06	Group 1	Carbonaceous clayey silt	Microbialite chimneys	McCormack et al., (2019)
	Schweizer 1975		-		9.60	28.08	164.2	0.190	7.16	37.8	0.001	0.04				Stockhecke et al., (2014)
	Irion 1973		-		9.90	26.87	155.2	0.074	9.88	133.8	0.0005	0.06				Kempe et al., (1991)
Lake Clifton	Moore 1987	Yalgorup lakes, (Australia)	S1, fig 8A, Table 2, F12	Coastal, hyposaline lagoon	-	16.83	1.71	18.999	101.81	5.4	11.111	70.65	Group 4	Peloids, Micrite mud Skeletal sands	Thrombolites	Burne 1987; et al., 2014
	Moore 1993		T3 (0m depth)		8.96	70	2.599	13.658	62.57	4.6	5.255	29.33				Moore, 1983
Great Salt Lake	Domagolski et al., 1989	Bonneville Basin, Utah (USA)	GSL3 transect (0,15m depth)	Endorheic, hypersaline lake	8.5	84.34	6.5	5.988	14.98	2.5	0.921	3.23	Group 3	Ooids, oncoids	Thrombolites	Chidsey et al., 2015
	Jones 2009		Gilbert bay (1m depth)		-	221	7.6	9.431	-	0.0	1.241	1.24		Peloids	Stromatolites	Della Porta, 2015
	Della Porta 2015		Bridge Bay/ North Arm		8.4	270	8.4	-	-	-	-	-		Micrite mud	Microbial peloidal cements	Venin et al., 2018
	Hahl et al., 1965		Measured in 1959-60		-	490.64	5.35	15.918	662.52	41.6	2.975	126.81		Microbial pustular grains ('pop corn')	Capping microbial crusts	Bouton et al., 2019
Mono Lake	Newton 1994	Mono Basin, California (USA)	Mono 1980	Endorheic, saline, alkaline lake	9.7	87	196	0.165	2.55	15.5	0.001	0.0139	Group 1	Micron-sized aragonite flakes	Carbonate mounds and pinnacles	Newton 1994
	Domagolski et al., 1989		depth: 1m		9.5	92.72	630	0.514	3.20	6.2	0.001	0.0059			Clotted peloidal micrite	Connell and Dreiss, 1995; Della Porta, 2015
	Connel and Dreiss1995		MLK, 1992		9.8	113.93	414.6	0.185	3.05	16.5	0.0004	0.0078				Brasier et al., 2018
Kiritimati	Arp et al., 2012	Atoll of Kiritimati, Republic of Kiritibati (Central Pacific)	Lake 21 surface	Fresh to hypersaline atoll lagoon-lake	8.37	201.8	4.24	75.848	394.88	5.2	17.889	111.02	Group 4	Microbialite intraclasts Loose spherulite sands	Reticulate microbialites Microbial mat-related spherules	Arp et al., 2012
			Lake 21 porewater		7.16	187.5	4.25	71.357	349.78	4.9	16.790	99.09				
			Lake 2		7.95	170.82	3.64	76.846	324.26	4.2	21.112	110.19				
Rottnest	Bischoff et al., 2020	Serpentine Lake (Western Australia)	October 2018, lake	Hypersaline lake	8.10	312.5	2.6	38.600	528	13.7	14.846	217.92		-	Spherulitic microbialite	Bischoff et al., 2020
			October 2019, lake		7.83	373.58	2.9	47.800	617.8	12.9	16.483	229.52				
														Summary crystal types		
Experiments	Tutolo and Tosca 2018	-	Run B	Saline alkaline synthetic solution	10.13	27.81	112	0.001	0.0004	0.3	0.00001	0.00001	Group 1	Dodecahedron-like single crystals,		
			Run E		10.14	30.13	112	0.002	0.0206	11.1	0.00002	0.0002		Elongated dipyramid single crystals,		
			Run F		10.14	30.13	112	0.0002	0.0100	50.1	0.000002	0.0001		Protruded dipyramid, and rhombic single crystals		
Experiments herein	Experiments herein	-	Experiment 1	Saline alkaline synthetic solution	12	2.08	127	17.515	17.151	1.0	0.138	0.27	Group 2	Polycrystalline, fibro-radial spherulites		
			Experiment 2		12	2.08	127	17.515	17.151	1.0	0.138	0.27		Polycrystalline, fibro-radial spherulites		
			Experiment 3		12	10.40	131	17.515	17.151	1.0	0.134	0.26		Polycrystalline, fibro-radial spherulites and dumbbell-shaped spherulites		
			Experiment 4		12	10.40	131	17.515	17.151	1.0	0.134	0.26		Rhombic single crystals		
Experiments	Beck and Andreassen, 2010	-	Experiment 13	Saline, alkaline synthetic solution	7	53.87	37.42	529.79	0.00	0.0	14.16	14.16	Group 4	Polycrystalline calcite spherulites		
Experiments	Tracy 1998	-	Trial 8	Saline alkaline synthetic solution	8.2	-	36.7	99.99	100.02	1.0	2.72	5.45	Group 2	Polycrystalline, fibro-radial calcite spherulites		
			Trial 16		8.2	0.7089	14.12	20.00	100.02	5.0	1.42	8.50				

TABLE 1

Wright, V.P., and Barnett, A. J. (2015). An abiotic model for the development of textures in some South Atlantic early Cretaceous lacustrine carbonates Cretaceous. *Geol. Soc. London, Spec. Publ.* 418, 1–11. https://doi.org/http://dx.doi.org/10.1144/SP418.3

Young, J. R., Davis, S. A., Bown, P. R., and Mann, S. (1999). Coccolith ultrastructure and biomineralisation. Journal of structural biology, 126(3), 195-215.

Zhou, L., and O'Brien, P. (2008). Mesocrystals: a new class of solid materials. *Small*, *4*(10), 1566-1574.

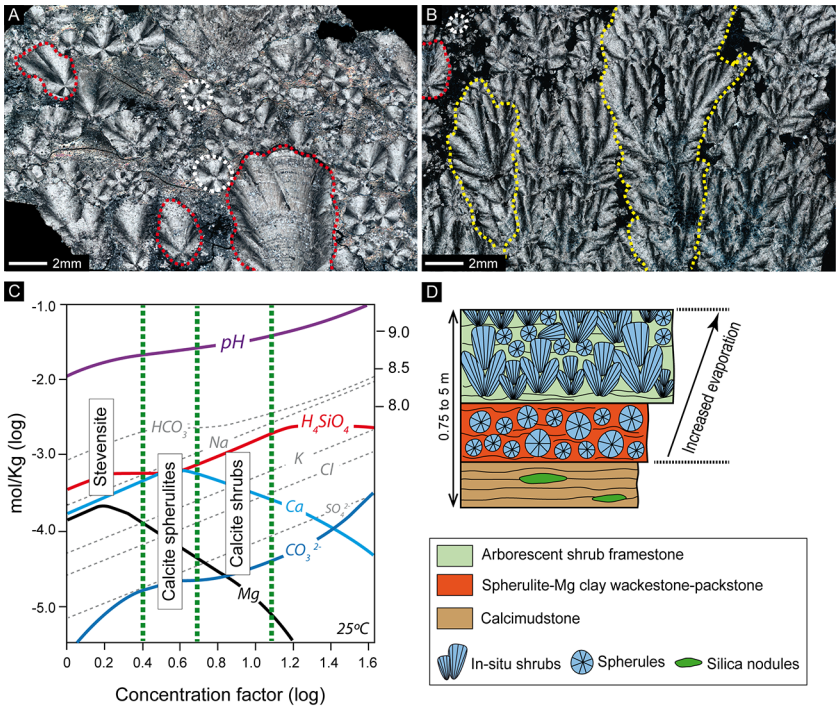

dep2_136_f1.tif

A

	Batch chemistry	Calcite petrographic features	Dimensions	Growth forms
Experiment 1	$SI_{calcite}$: 2.86 pH: 12 Alginic acid: 0mg/L NaCl: 2,08 g/L	- Polycrystalline, fibro-radial spherulites - Horizontal aggregation - Densely packed crusts	**Individual crystals**: up to 30µm-thick **Clusters**: up to 300µm-lenght	slide
Experiment 2	$SI_{calcite}$: 2.86 pH: 12 Alginic acid: 1mg/L NaCl: 2,08 g/L	- Polycrystalline, fibro-radial spherulites - Vertical aggregation - Tightly-packed shrubby aggregates	**Individual crystals**: up to 30µm-thick **Clusters**: up to 500µm-lenght	slide
Experiment 3	$SI_{calcite}$: 2.96 pH: 12 Alginic acid: 0 mg/L NaCl: 10,40 g/L	- Polycrystalline, fibro-radial spherulites - Dumbbell-shaped spherulites - Vertical and horizontal aggregation - Loosely-packed granular clusters	**Individual crystals**: up to 15µm-thick **Clusters**: up to 100µm-lenght	slide
Experiment 4	$SI_{calcite}$: 2.96 pH: 12 Alginic acid: 1 mg/L NaCl: 10,40 g/L	- Rhombic single-crystal structures - Horizontal aggregation - Imbricated twin clusters	**Individual crystals**: up to 15µm-thick **Clusters**: hundreds µm-lenght	slide

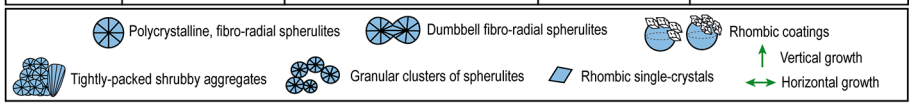

B

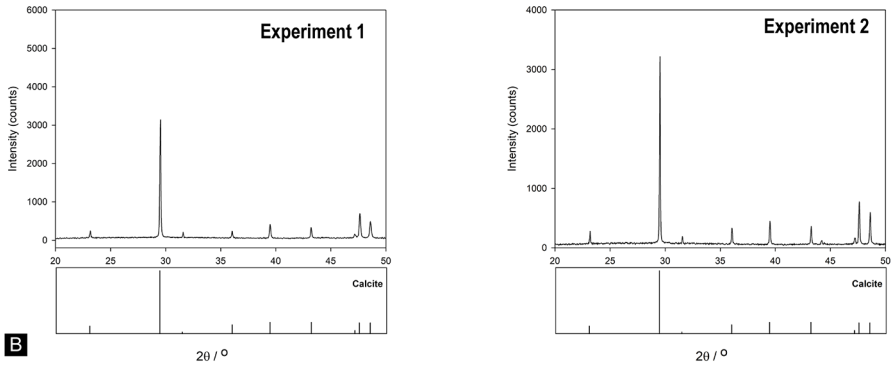

dep2_136_f2.tif

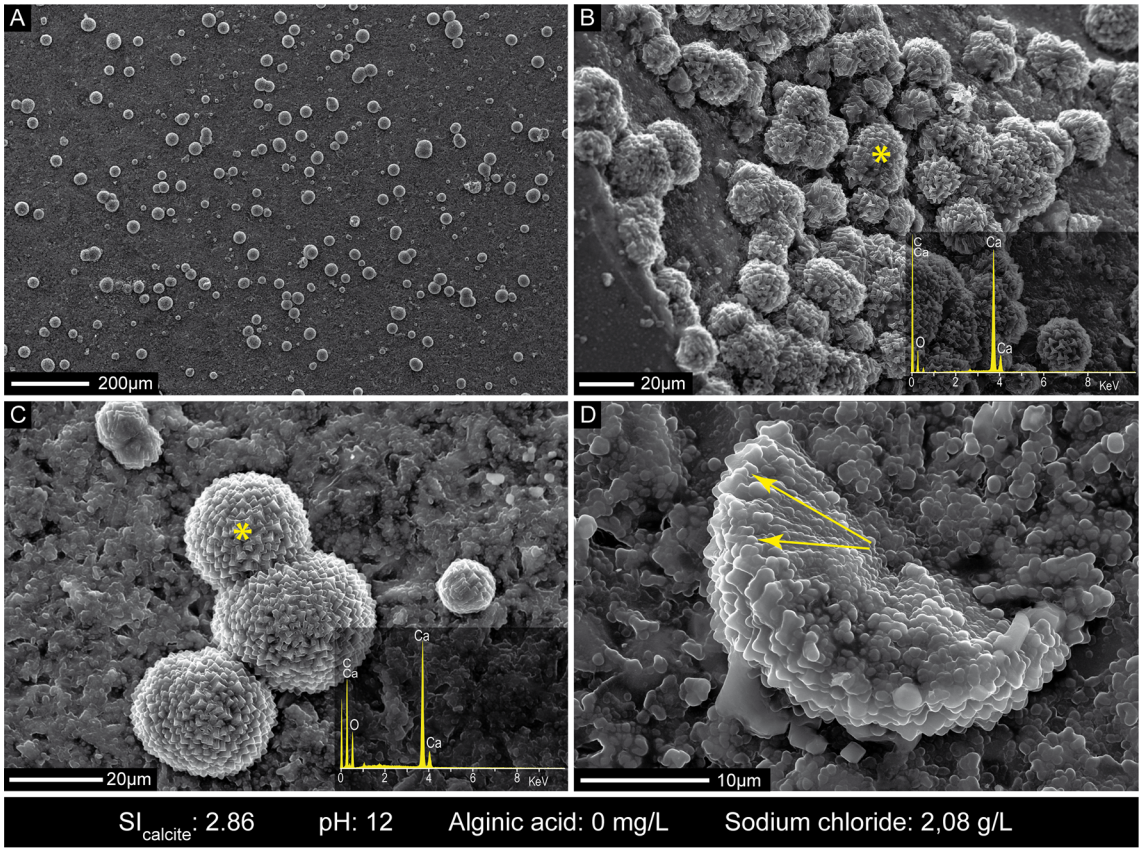

dep2_136_f3.tif

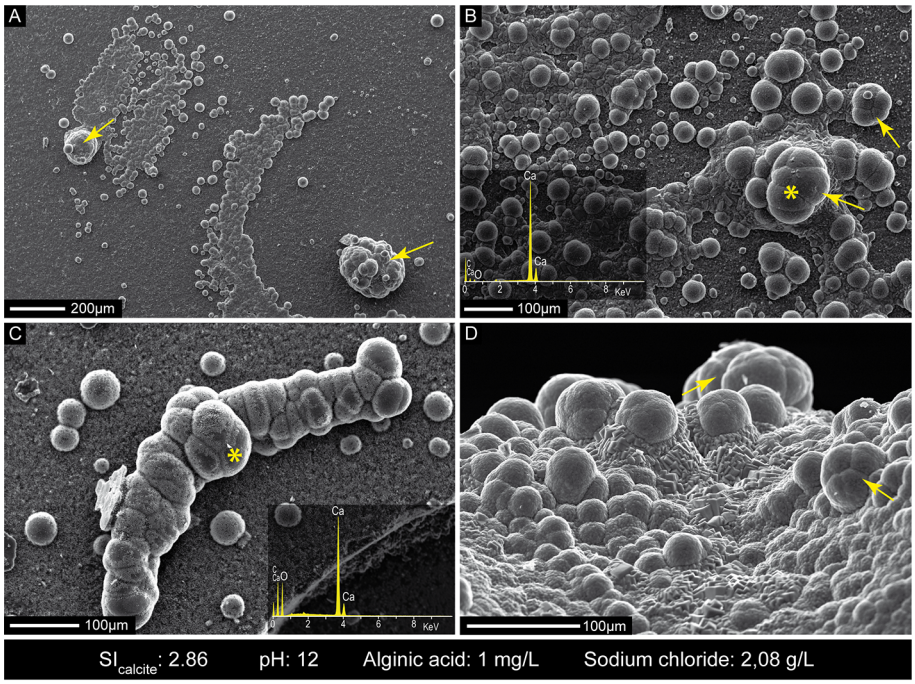

dep2_136_f4.tif

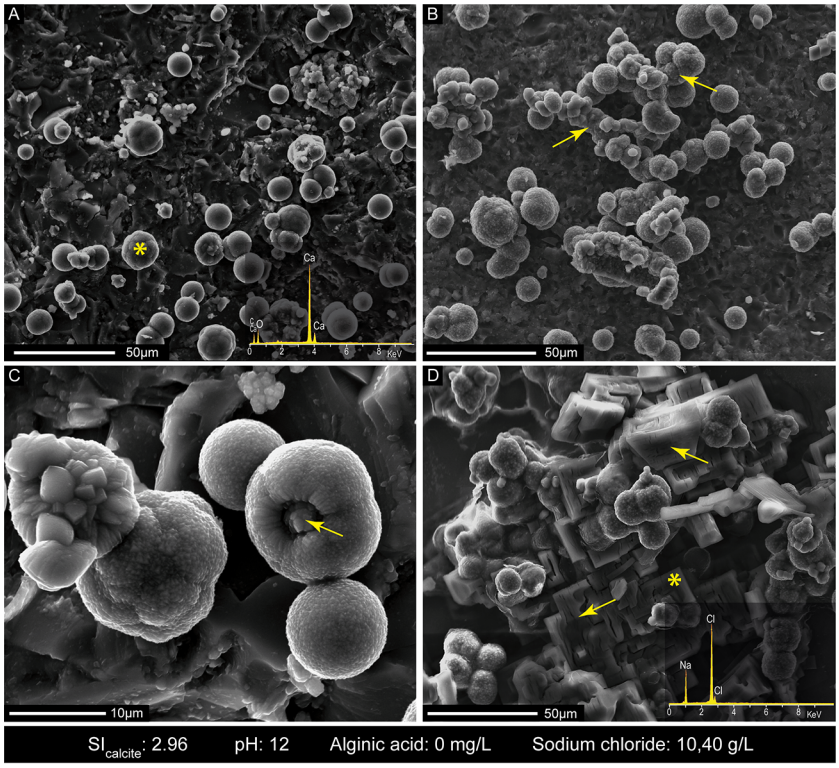

dep2_136_f5.tif

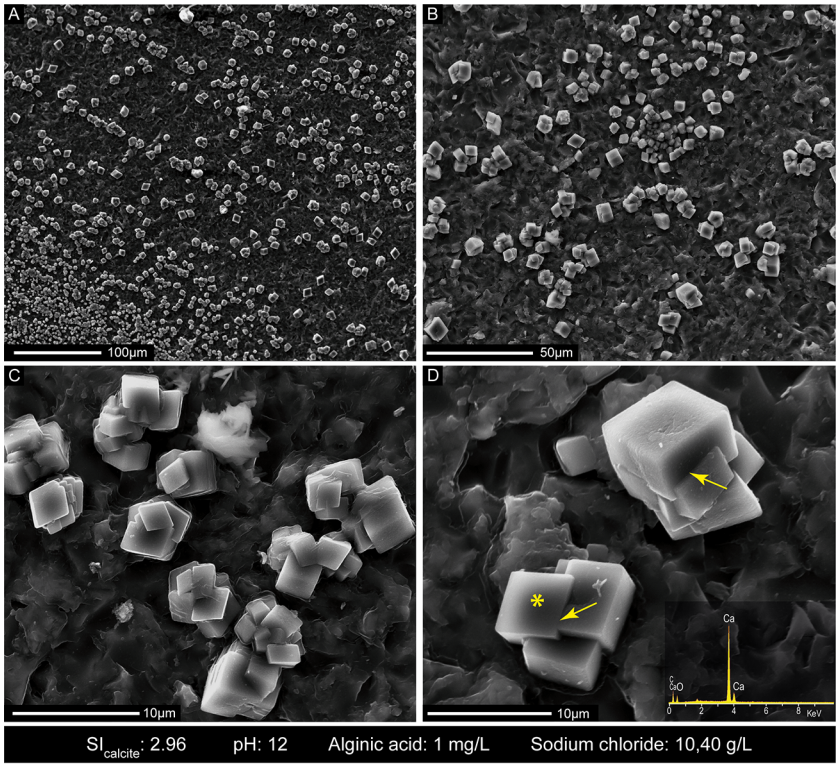

dep2_136_f6.tif

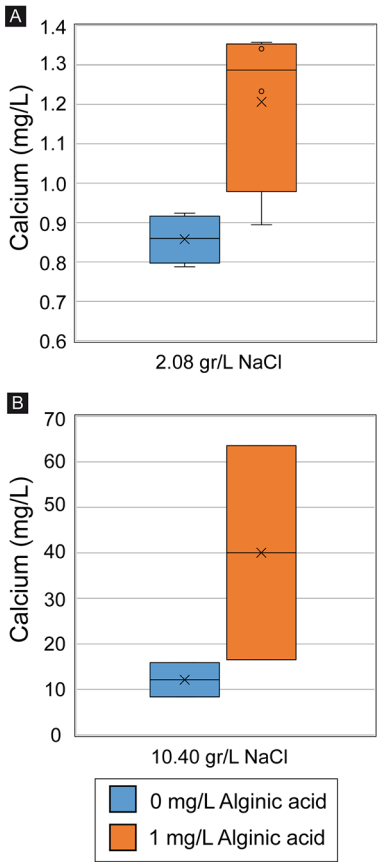

dep2_136_f7.tif

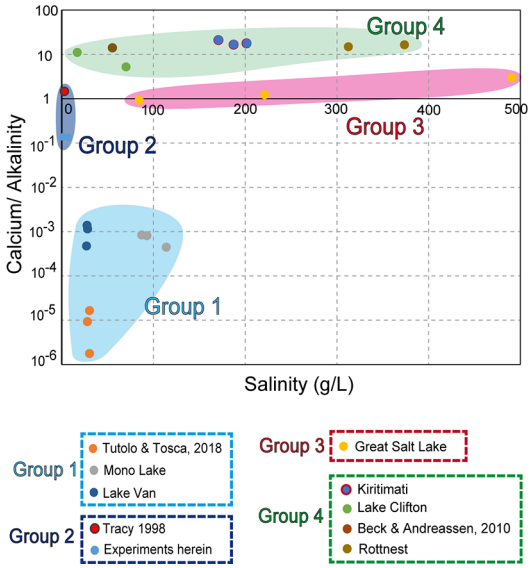

dep2_136_f8.tif

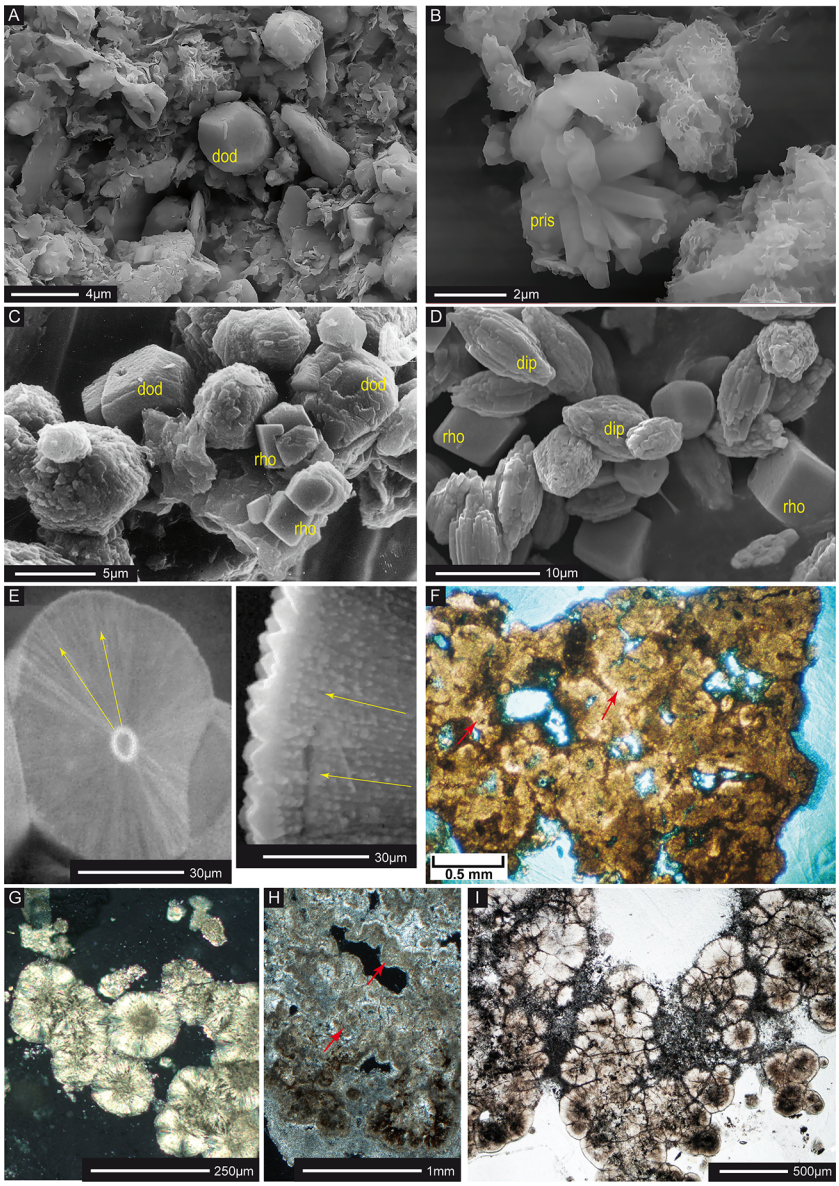

dep2_136_f9.tif

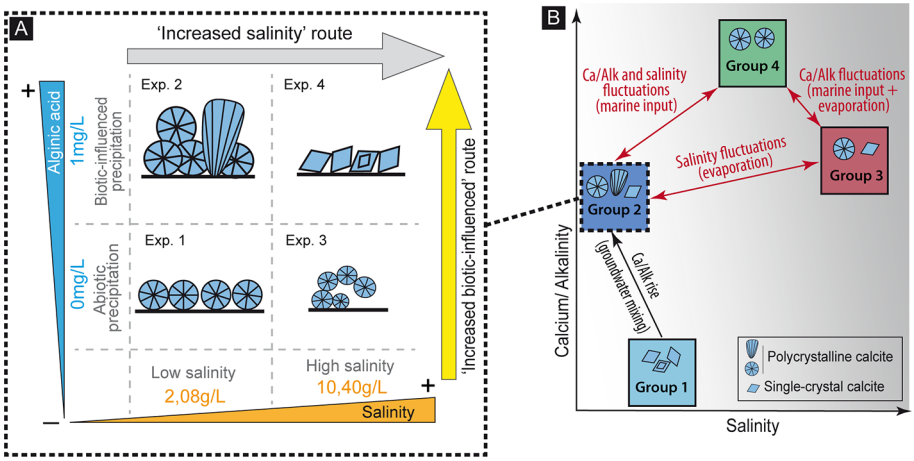

dep2_136_f10.tif

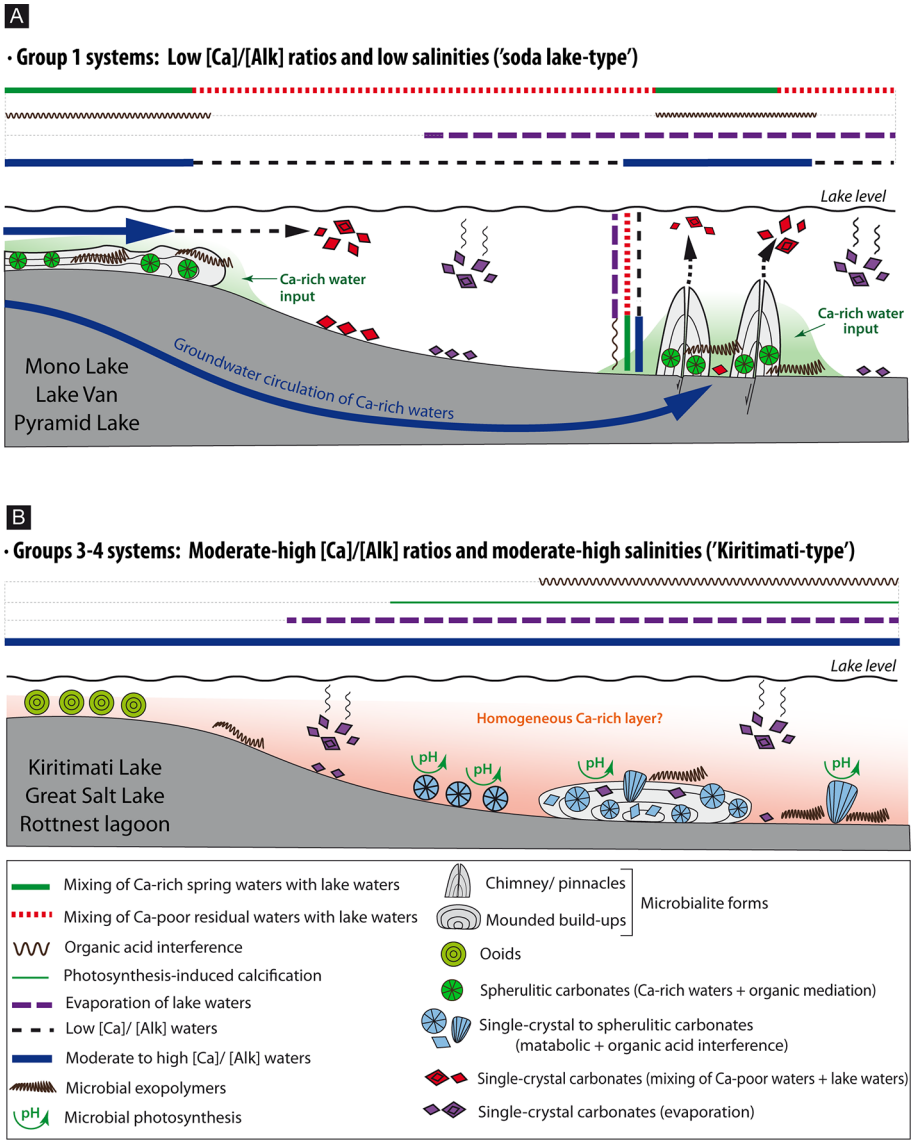

dep2_136_f11.tif